

Remeasuring the γ -decay branching ratio of the Hoyle state

W. Paulsen,^{1,*} K. C. W. Li,¹ S. Siem,¹ V. W. Ingeberg,¹ A. C. Larsen,¹ T. K. Eriksen,¹
H. C. Berg,^{1,†} M. M. Bjørøen,¹ B. J. Coombes,² J.T.H. Dowie,² F. W. Furmyr,¹
F. L. B. Garrote,¹ D. Gjestvang,¹ A. Görgen,¹ T. Kibédi,² M. Markova,¹
V. Modamio,¹ E. Sahin,¹ A. E. Stuchbery,² G. M. Tveten,¹ and V. M. Valsdóttir¹

¹*Department of Physics, University of Oslo, N-0316 Oslo, Norway*

²*Department of Nuclear Physics and Accelerator Applications,
Research School of Physics, The Australian National University,
Canberra, Australian Capital Territory 2601, Australia*

(Dated: June 4, 2024)

Background: The radiative branching ratio of the Hoyle state is crucial to estimate the triple- α reaction rate in stellar environments at medium temperatures of $T = 0.1$ to 2 GK. Knowledge of the γ -decay channel is critical as this is the dominant radiative decay channel for the Hoyle state. A recent study by Kibédi *et al.* [Phys. Rev. Lett. **125**, 182701 (2020)] has challenged our understanding of this astrophysically significant branching ratio and its constraints.

Purpose: Perform a new measurement of the γ -decay branching ratio of the Hoyle state to deduce the radiative branching ratio of the Hoyle state. An additional objective was to independently verify aspects of the aforementioned measurement conducted by Kibédi *et al.*

Method: For the primary experiment of this work the Hoyle state was populated by the $^{12}\text{C}(p,p')$ reaction at 10.8 MeV at the Oslo Cyclotron Laboratory. The γ -decay branching ratio was deduced through triple-coincidence events, each consisting of a proton ejectile corresponding to the 0_2^+ Hoyle state, and the subsequent cascade of 3.21 MeV and 4.44 MeV γ -rays. To verify the analysis, a surrogate γ -ray cascade from the 0_2^+ state in ^{28}Si was also studied. Following the same methodology an independent analysis of the 2014 data published by Kibédi *et al.* [Phys. Rev. Lett. **125**, 182701 (2020)] has been carried out.

Results: In the main experiment of this work, a γ -decay branching ratio of the Hoyle state of $\Gamma_{\gamma}^{E2}/\Gamma = 4.0(4) \times 10^{-4}$ was determined, yielding a corresponding radiative branching ratio of $\Gamma_{\text{rad}}/\Gamma = 4.1(4) \times 10^{-4}$. For the independent reanalysis of the 2014 data published by Kibédi *et al.* [Phys. Rev. Lett. **125**, 182701 (2020)], the discrepantly large branching ratio was reproduced.

Conclusions: The radiative branching ratio of the Hoyle state reported in this work is in agreement with several recent studies, as well as the previously adopted ENSDF average of $\Gamma_{\text{rad}}/\Gamma = 4.16(11) \times 10^{-4}$. Aspects of the analysis performed by Kibédi *et al.* were verified in this work. The source of discrepancy between the results of this work and that of Kibédi *et al.* could not be determined. Further independent and innovative studies for the radiative width of the Hoyle state will substantiate whether the discrepant result by Kibédi *et al.* should be excluded from future evaluations.

I. INTRODUCTION

The production of ^{12}C through the triple- α reaction is a fundamental process to our understanding of stellar nucleosynthesis (see Refs. [1–3] for further discussions). At medium temperatures between 0.1–2 GK, the triple- α reaction is predominantly mediated by the Hoyle state: the 0_2^+ resonance of ^{12}C at $E_x = 7.65407(19)$ MeV [4]. The existence of this resonance was first proposed by Fred Hoyle [5] and was first experimentally observed by Dunbar *et al.* [6]. The Hoyle state also plays a fundamental role in our understanding of nuclear clustering and its theoretical calculation remains a crucial test for the development of nuclear models [3, 7]. As such, the properties of the Hoyle state continue to be of tremendous interest for the scientific community, both theoretically and experimentally.

Accurate evaluations for the triple- α reaction rate are important to correctly model the subsequent stellar nucleosynthesis. At low temperatures below 0.1 GK, the direct mechanism dominates the triple- α reaction. At higher temperatures beyond 1 GK, there is significant uncertainty in the contributions to the triple- α reaction due to the presence of complex, broad resonance structures [8, 9] as well as extremely rare radiative decay branches [10, 11]. In contrast to the low- and high-temperature regimes, the medium-temperature regime between 0.1 and 2 GK has generally been understood to be well constrained [4, 12]. Specifically, it is the nuclear properties of the Hoyle state which directly determine the triple- α reaction rate at medium-temperatures and as such, accurate knowledge of these properties is crucial.

A recent measurement by Kibédi *et al.* [13] has challenged our understanding for the crucial radiative branching ratio of the Hoyle state, with reported value of $\Gamma_{\text{rad}}/\Gamma = 6.2(6) \times 10^{-4}$. This value is highly discrepant with the adopted value of $\Gamma_{\text{rad}}/\Gamma = 4.16(11) \times 10^{-4}$ given by Kelley *et al.* [4]. Given the astrophysical importance of the Hoyle state, the result of Ref. [13] has trig-

* wanja.paulsen@fys.uio.no

† Current address: Facility for Rare Isotope Beams, 640 S Shaw Ln, East Lansing, MI 48824, USA

gered many further investigations and this work presents an effort to remeasure the γ -decay and radiative branching ratios of the Hoyle state.

The radiative width of the Hoyle state cannot be measured directly, but it can be deduced indirectly with three independently measured quantities as

$$\Gamma_{\text{rad}} = \left[\frac{\Gamma_{\text{rad}}}{\Gamma} \right] \times \left[\frac{\Gamma}{\Gamma_{\pi}^{E0}} \right] \times [\Gamma_{\pi}^{E0}]. \quad (1)$$

The current recommended value for the radiative width of the Hoyle state is $\Gamma_{\text{rad}} = 3.81(39)$ meV [4], with an uncertainty of about 10%. The most precise term in Eq. 1 is $\Gamma_{\text{rad}}/\Gamma$, which can be expressed as

$$\frac{\Gamma_{\text{rad}}}{\Gamma} = \frac{\Gamma_{\gamma}^{E2} (1 + \alpha_{\text{tot}}) + \Gamma_{\pi}^{E0}}{\Gamma}, \quad (2)$$

where α_{tot} is the theoretical total $E2$ conversion coefficient and Γ_{π}^{E0}/Γ is the partial $E0$ pair decay width. This work reports a new measurement of $\Gamma_{\gamma}^{E2}/\Gamma$, which is deduced by measuring the γ -decay branching ratio of the Hoyle state. This rare decay mode from the Hoyle state corresponds to an $E2$ - $E2$ γ -ray cascade that proceeds through the first-excited 2_1^+ state to the ground state. Such events were observed as proton- γ - γ coincidences, corresponding to proton ejectiles having populated the Hoyle state, as well as the emission of 3.21 and 4.44 MeV γ rays of the following $E2$ - $E2$ γ -ray cascade. The $\Gamma_{\gamma}^{E2}/\Gamma$ branching ratio can be expressed as

$$\frac{\Gamma_{\gamma}^{7.65}}{\Gamma} = \frac{N_{020}^{7.65}}{N_{\text{inclusive}}^{7.65} \times \epsilon_{3.21} \times \epsilon_{4.44} \times c_{\text{det}} \times W_{020}^{7.65}}, \quad (3)$$

where $N_{020}^{7.65}$ is the amount of observed triple coincidences from the Hoyle state at 7.65 MeV as single-transition photopeaks and $N_{\text{inclusive}}^{7.65}$ is the inclusive amount of protons populating the Hoyle state. $\epsilon_{3.21}$ and $\epsilon_{4.44}$ are the respective $E_{\gamma} = 3.21$ and $E_{\gamma} = 4.44$ MeV full-energy photopeak efficiencies (per detector) for the $E2$ - $E2$ γ -ray cascade from the Hoyle state. $W_{020}^{7.65}$ is the angular correlation correction factor for the two γ rays and $c_{\text{det}} = n_{\text{det}}(n_{\text{det}} - 1)$ is a combinatorial factor, where n_{det} is the total number of γ -ray detectors in the setup.

II. EXPERIMENTAL APPARATUS

Three experiments were performed in this study, with the experimental conditions summarized in Table I. In this work, the primary experiment to study the 0_2^+ Hoyle state was performed in 2019 (Sec. II A). An additional experiment in 2020 was performed to study the decay of the 0_2^+ state in ^{28}Si as a surrogate for that of the Hoyle state (Sec. II B). Data from this 2020 experiment was used to obtain efficiencies and validate the analysis methodology employed in this work. Finally, an independent analysis of the data published by Kibédi *et al.* [13] was performed in this work (Sec. II C).

A. $^{12}\text{C}(p, p')$ with $E_p = 10.8$ MeV performed in 2019

The Hoyle state was populated through inelastic proton scattering on a $^{\text{nat}}\text{C}$ target with an areal density of $180 \mu\text{g}/\text{cm}^2$. The beam energy was $E_p \approx 10.8$ MeV and was delivered with a current of 2–6 nA by the MC-35 Scanditronix cyclotron at the Oslo Cyclotron Laboratory (OCL). Ejectiles were detected using the Silicon Ring (SiRi) particle-telescope system, consisting of eight trapezoidal modules mounted at a distance of ≈ 5 cm from the target [14]. These modules covered a polar-angle range of 126° – 140° , with $\approx 2^\circ$ being subtended by each of the eight rings acting as the front ΔE -layer. The thickness of the ΔE and E detectors are approximately 130 and 1550 μm , respectively [14]. The coincident γ -rays decays were detected with the OSCAR multidetector system [16]. The large-volume $\text{LaBr}_3(\text{Ce})$ detectors of OSCAR were configured at closest possible distance of ≈ 16.3 cm to the target, each detector subtending a solid angle of $\approx 1.9\%$ of 4π . Events were triggered by signals in the ΔE detectors, with the time-to-digital (TDC) values from coincidentally triggered $\text{LaBr}_3(\text{Ce})$ detectors being recorded relative to that of the detected proton.

B. $^{28}\text{Si}(p, p')$ with $E_p = 16.0$ MeV performed in 2020

In 2020 a $140 \mu\text{g}/\text{cm}^2$ -thick SiO_2 target with a $30 \mu\text{g}/\text{cm}^2$ -thick $^{\text{nat}}\text{C}$ backing was employed to study states in ^{28}Si to test the background subtraction method and obtain in-beam efficiencies relevant for Eq. 3. Events were triggered by signals in the ΔE detectors of the SiRi particle-telescope system, configured to a polar-angle range of 126° – 140° . The coincident γ rays were detected with the OSCAR multidetector system.

C. $^{12}\text{C}(p, p')$ with $E_p = 10.7$ MeV performed in 2014

The data from this experiment were previously published by Kibédi *et al.* [13]. The Hoyle state was populated through inelastic proton scattering on a $^{\text{nat}}\text{C}$ target with an areal density of $180 \mu\text{g}/\text{cm}^2$ using a beam energy of 10.7 MeV. Other targets were also employed in this 2014 measurement, but the corresponding data were not analyzed in this work. Events were triggered by signals in the ΔE detectors of the SiRi particle-telescope system, configured to a polar-angle range of 126° – 140° . The coincident γ rays were detected with the CACTUS multidetector system [15]. The large-volume $\text{NaI}(\text{Ti})$ detectors of CACTUS were configured at ≈ 22 cm from the target, collimated with 10 cm of lead, with each detector subtending a solid angle of $\approx 0.63\%$ of 4π .

TABLE I. A summary of the experimental conditions of the three measurements studied in this work. The primary experiment of this work was the $^{12}\text{C}(p, p')$ measurement performed in 2019.

	$^{12}\text{C}(p, p')$ with $E_p = 10.7$ MeV performed in 2014 [13]	$^{12}\text{C}(p, p')$ with $E_p = 10.8$ MeV performed in 2019	$^{28}\text{Si}(p, p')$ with $E_p = 16.0$ MeV performed in 2020
Ejectile detector	SiRi ($\theta = 126.0\text{--}140.0^\circ$) [14]	SiRi ($\theta = 126.0\text{--}140.0^\circ$) [14]	SiRi ($\theta = 126.0\text{--}140.0^\circ$) [14]
γ -ray detector	NaI(Tl) ($n_{\text{det}} = 26$) [15]	LaBr ₃ (Ce) ($n_{\text{det}} = 30$) [16]	LaBr ₃ (Ce) ($n_{\text{det}} = 30$) [16]
Total γ -ray efficiency (1.3 MeV)	$\approx 14.1\%$	$\approx 56.0\%$	$\approx 56.0\%$
Distance from target	22.0 cm	16.3 cm	16.3 cm
Target	$^{\text{nat}}\text{C}$ (180 $\mu\text{g}/\text{cm}^2$)	$^{\text{nat}}\text{C}$ (180 $\mu\text{g}/\text{cm}^2$)	SiO ₂ (140 $\mu\text{g}/\text{cm}^2$) with $^{\text{nat}}\text{C}$ (30 $\mu\text{g}/\text{cm}^2$) backing

III. DATA ANALYSIS

For the primary experiment of this work, the data analysis methods are explained in detail (Sec. III A). The same methodology is employed in the consistent analyses of the 2020 and 2014 experiments, which are presented in Secs. A 1 and III B, respectively.

The analysis method conducted on the data obtained from the 2019 and 2020 experiments was performed on the data obtained in 2014 (published in Ref. [13]), with the goal of independently verifying aspects of the analysis performed in Ref. [13].

A. $^{12}\text{C}(p, p')$ with $E_p = 10.8$ MeV performed in 2019

For the $^{\text{nat}}\text{C}(p, p')$ reaction, the energy depositions in the ΔE detector of SiRi for angles $\theta_{\text{lab}} = 126^\circ\text{--}140^\circ$ from scattered protons are shown in Fig. 1. Only the ΔE signal from SiRi was employed to gate on the Hoyle state as the corresponding proton ejectiles were stopped in the ΔE detector. The Hoyle/ 2_1^+ population ratio of this 2019 experiment is different to that of the 2014 experiment [13] due to the lower $E_p = 10.7$ MeV beam energy for the latter case. For the 2014 experiment [13], the Hoyle/ 2_1^+ population ratio is in agreement with the study by Cook *et al.* [17] (measured between $E_p \approx 10.2\text{--}10.7$ MeV). A linear extrapolation of the Hoyle/ 2_1^+ population ratios in Ref. [17] up to $E_p = 10.8$ MeV is in good agreement with that observed in this 2019 measurement (the primary experiment of this work). Due to the reaction kinematics, the kinetic energy of the proton is highly dependent on the polar angle between the detector ring and the beam detection axis. Because of the resultant kinematic smearing across each subtended angle, the data from each ring is fitted separately. The ordering of the 0_1^+ , 2_1^+ and 0_2^+ peaks does not follow that of the corresponding excitation energies as the proton ejectiles corresponding to Hoyle state are stopped in the ΔE layer of SiRi. In contrast, the ejectiles corresponding to the lower-lying 2_1^+ and 0_1^+ states do penetrate the ΔE layer and are stopped in the E detector. Due to this complex kinematic behavior in

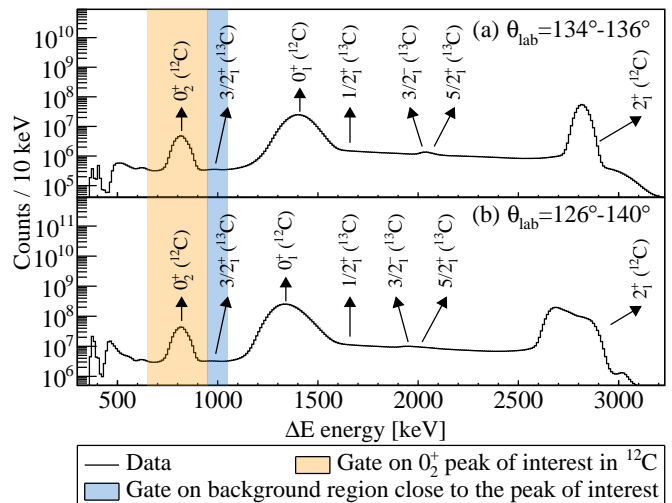


FIG. 1. (a) ΔE energy spectrum of inelastically scattered proton ejectiles, detected at $\theta_{\text{lab}} = 134^\circ\text{--}136^\circ$ with SiRi from the measurement performed in 2019. The orange shaded area denotes the energy gate employed for the 0_2^+ Hoyle state. The blue shaded area denotes the energy gate employed for the background gated analysis, as explained in Appendix A 2. The total projection of all angles of SiRi ($\theta_{\text{lab}} = 126^\circ\text{--}140^\circ$) is shown in panel (b). The energy calibration for this data was conducted under the assumption of no dead layer in the particle detector (see text for details).

the ΔE of SiRi, and variations in the thickness of the ΔE dead layer, the calibration was performed under the assumption that no dead layer exists. This assumption is valid because the absolute energies of the proton ejectiles do not affect the analysis; the ΔE spectra are simply used to select for events from the state of interest, such as Hoyle-state events and to estimate the background underneath the peak of interest. A few weakly populated states from ^{13}C are also observed in the inclusive spectra, however, the decays from these states do not interfere with the analysis of the Hoyle state.

In this work, the triple-coincidence events ($p\text{-}\gamma\text{-}\gamma$) of interest to study the γ -decay branching ratio of the Hoyle state consist of a proton exciting the 0_2^+ state and two γ rays with energies $E_\gamma = 3.21$ and 4.44 MeV. To se-

lect the correlated γ -ray decays, a timing matrix is employed. Fig. 2 shows the time difference between detected ΔE proton ejectiles corresponding to the Hoyle state, and the LaBr₃(Ce) timing signals corresponding to $E_\gamma = 3.21$ MeV and $E_\gamma = 4.44$ MeV. The time locus at

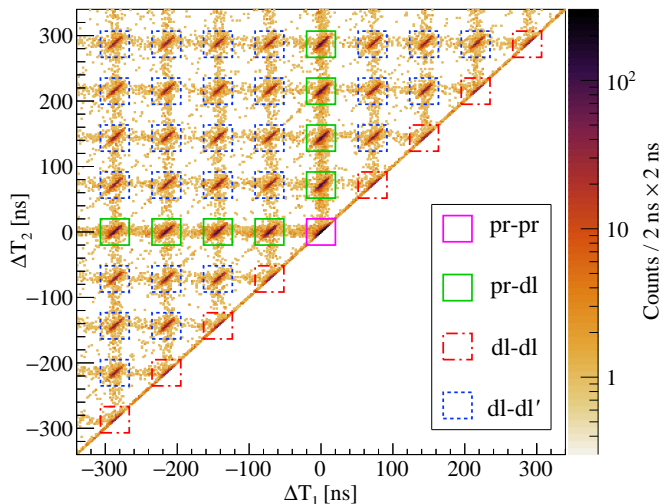


FIG. 2. Time differences between protons populating the Hoyle state and two γ rays with $E_\gamma = 3.21$ MeV and $E_\gamma = 4.44$ MeV, from the experiment performed in 2019. The matrix is sorted so that the largest of the two measured times is along the y-axis. The colored boxes denote the different timing gates used for the analysis. See text for an explanation of coincidence events.

$\Delta T_1 \approx \Delta T_2 \approx 0$ ns, denoted pr-pr, corresponds to p - γ - γ coincidences where both γ rays are detected in prompt coincidence with the proton ejectile corresponding to the Hoyle state. To select for correlated p - γ - γ events corresponding to the Hoyle state, a gate was placed around the pr-pr time locus. However, within this pr-pr time locus, uncorrelated events are also present and these background components can be determined by gating on other timing loci.

The first of these uncorrelated components within the p - γ - γ events is where only one of the two detected γ rays is correlated with the detected ejectile corresponding to the Hoyle state. To estimate this component, which we denote pr-dl, we gate on events where only one γ ray is in prompt coincidence, whilst the other is delayed by at least one beam pulse. The second uncorrelated component, where both γ rays are correlated with each other, but are both uncorrelated with the proton (e.g., from a delayed beam pulse), is denoted dl-dl. Finally, the component for the completely random background, where none of the particles are correlated in time, is denoted dl-dl'. The square (40 ns-wide) gates for these pr-dl, dl-dl and dl-dl' components are presented in Fig. 2. In order to increase the statistics for the estimation of these various background yield components, multiple pr-dl, dl-dl and dl-dl' loci are selected up to four beam pulses away from the pr-pr time locus (see Fig. 2). These yields

are then normalized to the single pr-pr time locus. The background-subtracted yield for triple-coincidence events corresponding to the Hoyle state is thus determined as

$$N_{020}^{7.65} = N_{\text{pr-pr}} - N_{\text{pr-dl}} - N_{\text{dl-dl}} + N_{\text{dl-dl}'}, \quad (4)$$

where $N_{020}^{7.65}$ is employed in Eq. 3. The reason why the $N_{\text{dl-dl}'}$ is added, is because this completely random background component is subtracted twice through the $N_{\text{pr-dl}}$ and $N_{\text{dl-dl}}$ components, which each contain this completely random background. Fig. 3(a) presents the γ - γ matrix gated on the pr-pr time locus. The red, dashed horizontal lines correspond to the 3σ gate employed on the $E_\gamma = 4.44$ MeV γ -ray in the Hoyle-state cascade. To obtain the background-subtracted triple-coincidence yield ($N_{020}^{7.65}$), the various components in Eq. 4 must be determined. The corresponding γ -ray spectra for the pr-pr, pr-dl, dl-dl and dl-dl' components are generated by gating on the γ - γ matrix (Fig. 3(a) as well as on the corresponding time loci in Fig. 2. To accurately fit the data, the spectra were simultaneously fitted to yield $\chi_{\text{red}}^2 = 0.92$, with the mean and experimental width of the peaks being shared parameters. The independent polynomial backgrounds (either first- or second-order) for each spectrum were simultaneously optimized in the fit analysis. This technique enables the fit parameters to be better constrained, particularly for the spectra with low statistics. Fig. 3(c)-(f) presents the fitted histograms corresponding to the pr-pr, pr-dl, dl-dl and dl-dl' components. An equivalent analysis to obtain the background-subtracted triple-coincidence yield $N_{020}^{7.65}$ was employed by gating on the summed- γ matrices, as in Fig. 4(a).

The gating technique employed here is similar to that in Ref. [13], however, there are some notable differences. The horizontal, red dashed lines correspond to the 3σ gate on the summed- γ energies, similar to that employed in Ref. [13]. The region in the blue dashed lines corresponds to the smooth Compton continuum (from the $E_\gamma = 4.44$ MeV γ -ray) which underlies the $E_\gamma = 3.21$ MeV peak of interest. The events of interest are those which are within either (or both) of the aforementioned red and blue dashed regions. The corresponding, simultaneously fitted histograms are presented in Fig. 4(c)-(f), yielding a global $\chi_{\text{red}}^2 = 1.01$.

B. $^{12}\text{C}(p, p')$ with $E_p = 10.7$ MeV performed in 2014

Similarly to the experiment performed in 2019 (which had a beam energy of $E_p = 10.8$ MeV, see Sec. III A), the beam energy of $E_p = 10.7$ MeV for this 2014 experiment resulted in the ejectile protons from the Hoyle state being stopped in the ΔE layer of SiRi. The same effect on the ordering of the 0_1^+ , 2_1^+ and 0_2^+ peaks (to not follow the corresponding excitation energy) was therefore also present. The energy calibration was performed under the assumption of no dead layer, as for the 2019 measurement (see Sec. III A). The energy depositions from

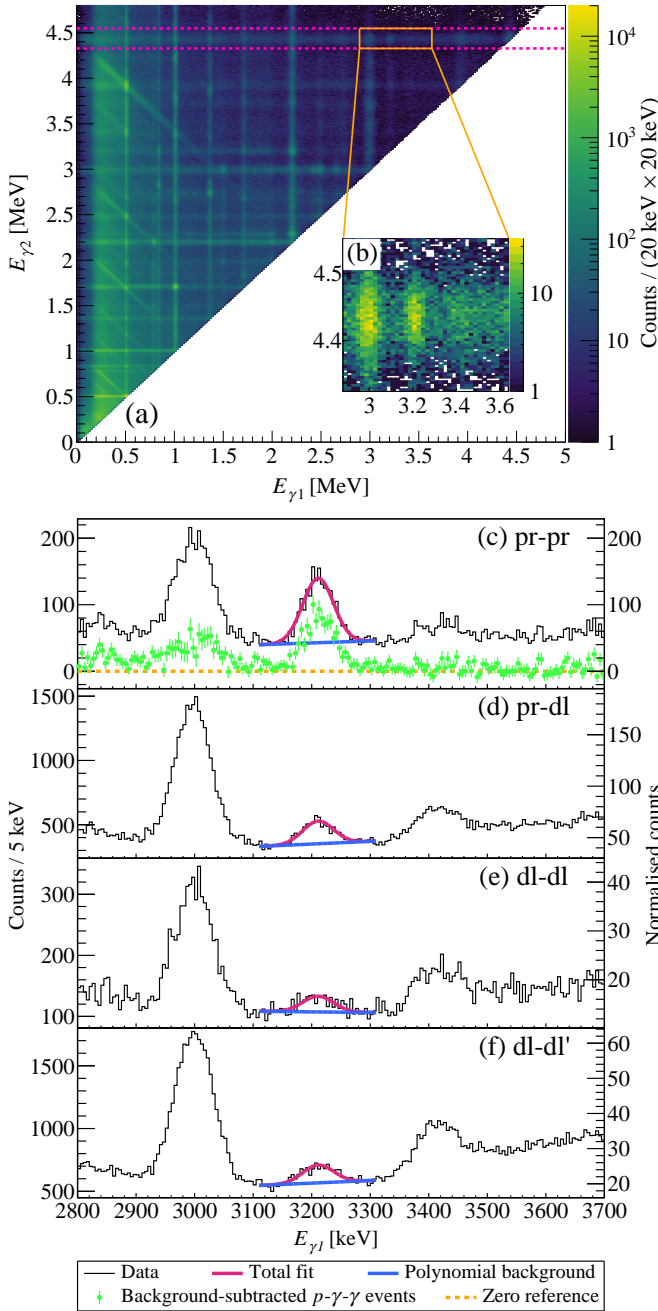


FIG. 3. (a) The γ - γ matrix (largest energy on the y-axis) gated on the pr-pr time locus (see Fig. 2) from the $^{12}\text{C}(p, p')$ measurement performed in 2019. A zoomed-in region, indicated with solid violet lines, is shown in panel (b). The horizontal, red dashed lines correspond to the 3σ gate on the summed- γ energies from the Hoyle state in ^{12}C , similar to that employed in Ref. [13]. The events of interest are those within the aforementioned red dashed region, with the projected spectra shown in panels (c)–(f) for the different time loci. The y-axis on the right side shows the normalized counts, accounting for the number of loci for each spectrum. The simultaneous fit yielded a global $\chi^2_{\text{red}} = 0.92$.

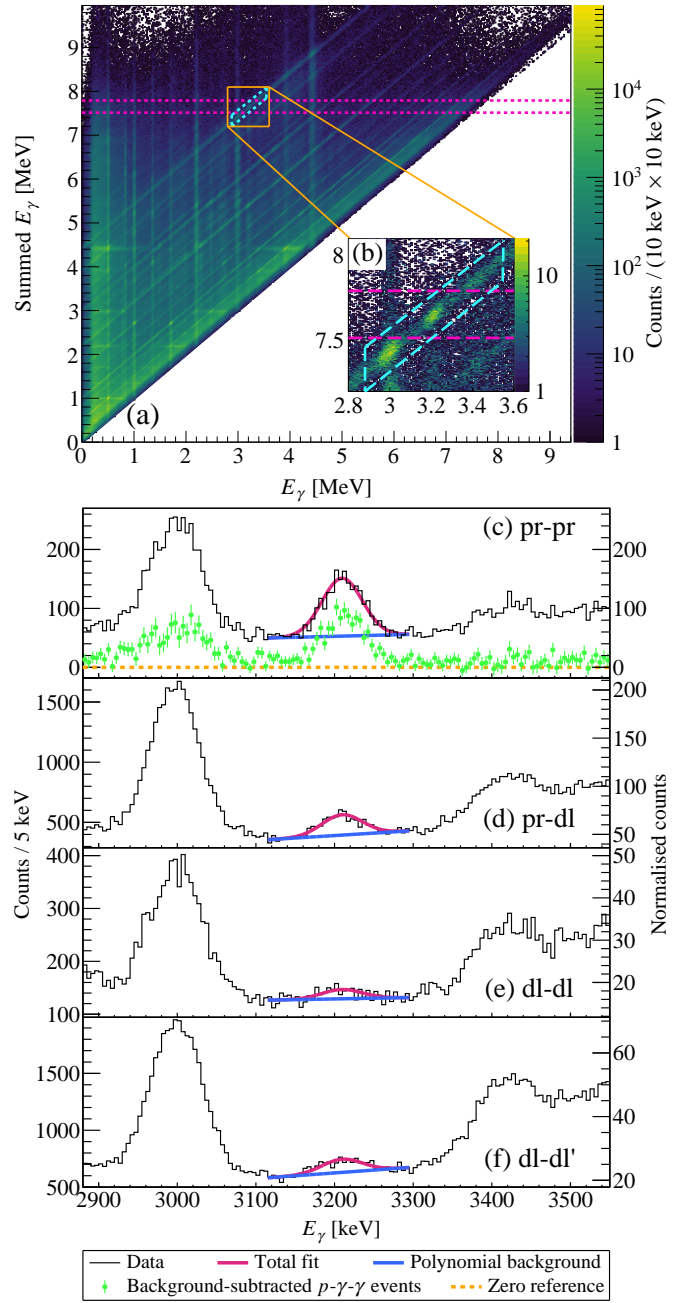


FIG. 4. (a) The summed- γ matrix gated on the pr-pr time locus (see Fig. 2) from the $^{12}\text{C}(p, p')$ measurement performed in 2019. A zoomed-in region, indicated with solid violet lines, is shown in panel (b). The horizontal, red dashed lines correspond to the 3σ gate on the summed- γ energies from the Hoyle state in ^{12}C , similar to that employed in Ref. [13]. The region in the blue dashed lines corresponds to the smooth Compton continuum (from the $E_\gamma = 4.44$ MeV γ -ray in coincidence with another $E_\gamma = 4.44$ MeV γ -ray) which underlies the $E_\gamma = 3.21$ MeV peak of interest. The events of interest are those which are within either (or both) of the aforementioned red and blue dashed regions, with the projected spectra shown in panels (c)–(f) for the different time loci. The y-axis on the right side shows the normalized counts, accounting for the number of loci for each spectrum. The simultaneous fit yielded a global $\chi^2_{\text{red}} = 1.01$.

scattered protons in the ΔE layer of SiRi are shown in Fig. 5. The orange shaded area shows the gate employed to obtain the triple-coincidence yield from the Hoyle state. The blue shaded area shows the gate employed for the background-gated analysis, as explained in Appendix A 4. Fig. 6 presents the time difference be-

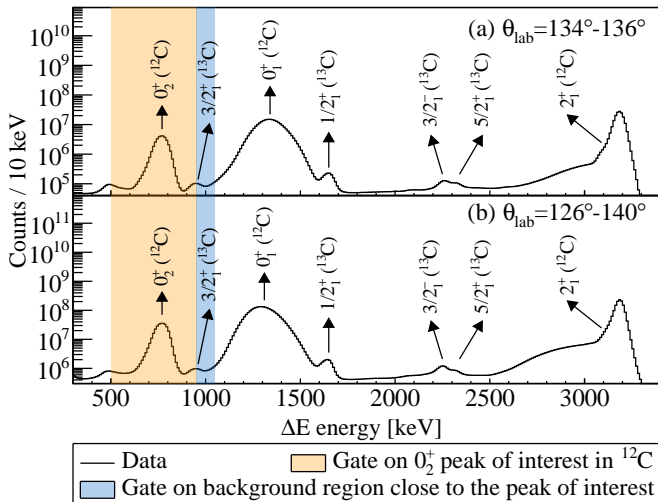


FIG. 5. (a) ΔE energy spectrum of inelastically scattered proton ejectiles, detected at $\theta_{\text{lab}} = 134^\circ\text{--}136^\circ$ with SiRi from the measurement performed in 2014. The orange shaded area denotes the energy gate employed for the 0_2^+ Hoyle state. The blue shaded area denotes the energy gate employed for the background gated analysis, as explained in Appendix A 2. The total projection of all angles of SiRi ($\theta_{\text{lab}} = 126^\circ\text{--}140^\circ$) is shown in panel (b). The energy calibration for this data was conducted under the assumption of no dead layer in the particle detector (see text for details).

tween the detected (ΔE) proton ejectile corresponding to the 0_2^+ Hoyle state, and the NaI(Tl) timing signals corresponding to $E_\gamma = 3.21$ MeV and $E_\gamma = 4.44$ MeV. In Fig. 7(a) the $\gamma\text{-}\gamma$ matrix gated on the pr-pr time locus is shown. The red, dashed horizontal lines correspond to the 3σ gate employed on the $E_\gamma = 4.44$ MeV γ -ray in the 0_2^+ Hoyle state cascade, with a zoomed-in region focused on the $E_\gamma = 3.21$ MeV and $E_\gamma = 4.44$ MeV coincidence locus shown in Fig. 7(b). The γ -ray spectra corresponding to these gated $\gamma\text{-}\gamma$ matrices (for the various time loci pr-pr, pr-dl, dl-dl and dl-dl'), the simultaneous fit is shown in Fig. 7(c)–(f). Due to the very clean signal in this experiment and the low statistics of the background components, a fit using maximum likelihood estimation was performed.

The summed- γ matrix gated on the pr-pr time locus is presented in Fig. 8(a). By gating on such summed- γ matrices for different timing loci, the corresponding triple-coincidence yields can be extracted. Fig. 8(c)–(f) presents the the simultaneous fit of these spectra, which was performed with maximum likelihood estimation due to the very low statistics of the various background components. The uncertainties of weakly populated peaks were conservatively estimated by adding (in quadrature)

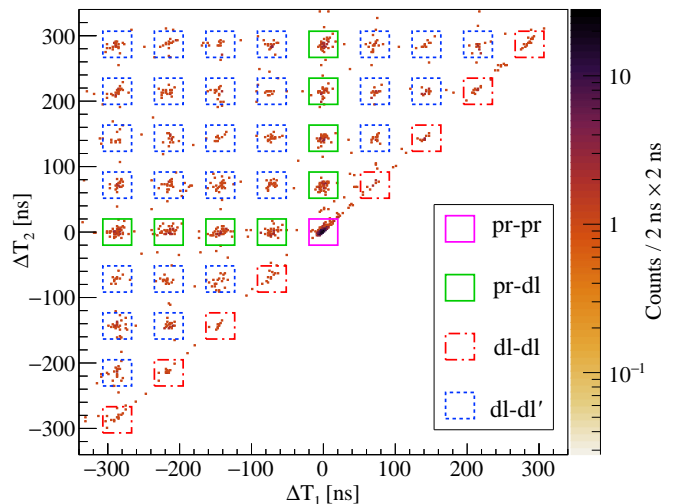


FIG. 6. Time differences between protons populating the Hoyle state and two γ rays with $E_{\gamma 1} = 3.21$ MeV and $E_{\gamma 2} = 4.44$ MeV, from the experiment performed in 2014. The matrix is sorted so the largest of the two timing values is along the y-axis. The colored boxes denote the different background gates used for the analysis. See text for explanation of coincidence events.

the statistical uncertainty of the histogram in the range of the peak.

C. Angular-correlation correction factors and efficiencies for OSCAR

This section explains the procedure to obtain the angular-correlation correction factors and γ -ray efficiencies for OSCAR, which are used in the measurements performed in 2019 and 2020 (see Table I for summary). For CACTUS used in the 2014 measurement [13], the procedure to obtain γ -ray efficiencies is explained in Appendix A 3 (see Table VII for a summary).

For OSCAR, used in the 2019 and 2020 measurements, in-beam data was employed together with a GEANT4 simulation developed by Zeiser *et al.* [16] to determine the absolute full-energy photopeak efficiencies ($\epsilon_{3.21}$ and $\epsilon_{4.44}$) and the angular correlation correction factor ($W_{020}^{7,65}$) in Eq. 3. The simulation enabled the response of the entire apparatus to be accounted for, e.g., attenuation from the spherically asymmetric scattering chamber. The corresponding γ -ray angular correlations in Fig. 9 were extracted with a simultaneous fitting procedure (analogous to Fig 3(c)–(f)) to reduce the fit uncertainties. These correlations were analyzed with fits of the form [18]

$$W(\theta) = \sum_{k=\text{even}}^{2L} A_k P_k(\cos\theta), \quad (5)$$

where P_k are the Legendre polynomials and L is the angular momentum of decay. To accurately account for the

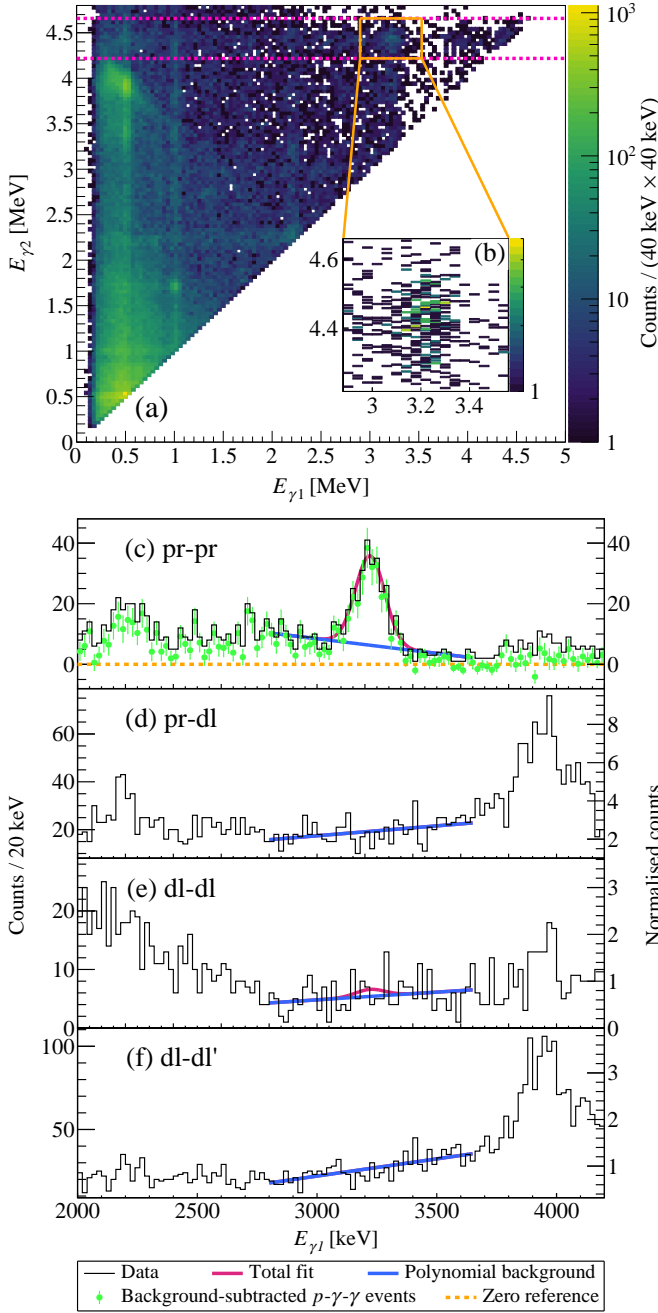


FIG. 7. (a) The γ - γ matrix (largest energy on the y-axis) gated on the pr-pr time locus (see Fig. 6) from the $^{12}\text{C}(p, p')$ measurement performed in 2014. A zoomed-in region, indicated with solid violet lines, is shown in panel (b). The horizontal, red dashed lines correspond to the 3σ gate on the summed- γ energies from the Hoyle state in ^{12}C , similar to that employed in Ref. [13]. The events of interest are those within the aforementioned red dashed region, with the projected spectra shown in panels (c)–(f) for the different time loci. The y-axis on the right side shows the normalized counts, accounting for the number of loci for each spectrum. The simultaneous fit yielded a global This simultaneous fit was performed with maximum likelihood estimation due to the very low statistics of the various background components.

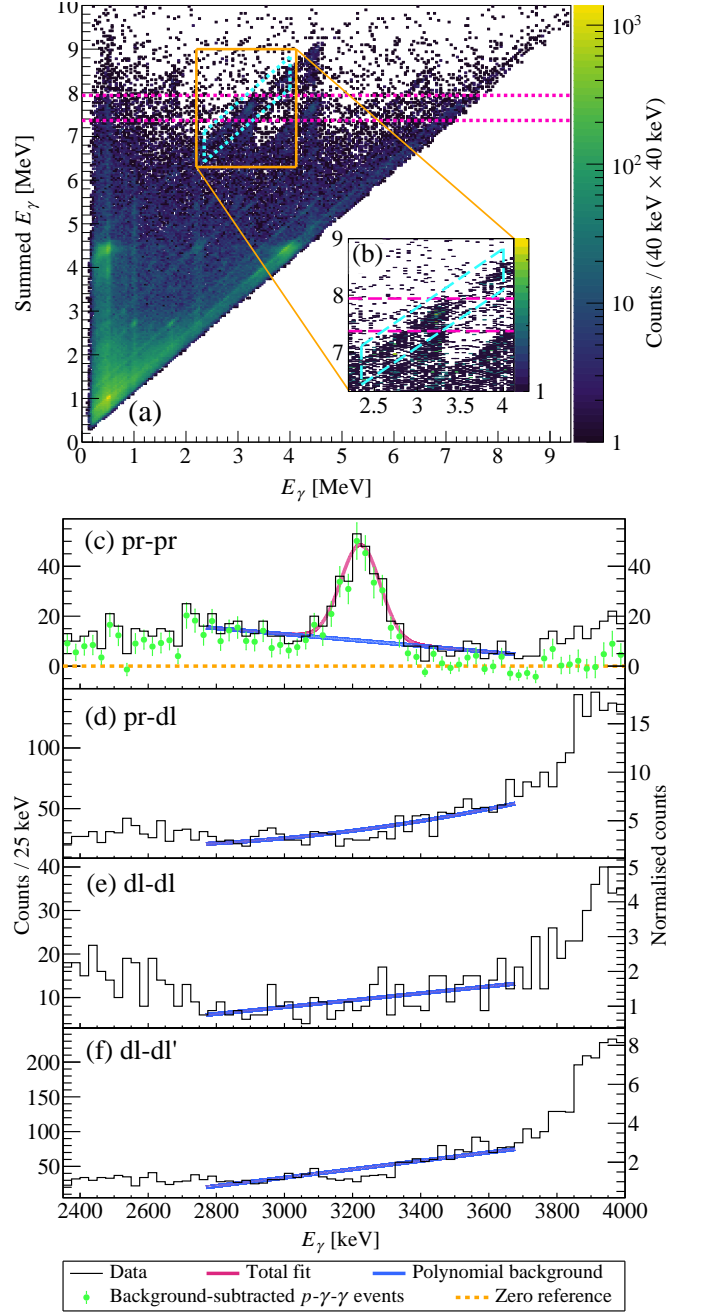


FIG. 8. (a) The summed- γ matrix gated on the pr-pr time locus (see Fig. 6) from the $^{12}\text{C}(p, p')$ measurement performed in 2014. A zoomed-in region, indicated with solid violet lines, is shown in panel (b). The horizontal, red dashed lines correspond to the 3σ gate on the summed- γ energies from the Hoyle state in ^{12}C , similar to that employed in Ref. [13]. The region in the blue dashed lines corresponds to the smooth Compton continuum (from the $E_\gamma = 4.44$ MeV γ -ray in coincidence with another $E_\gamma = 4.44$ MeV γ -ray) which underlies the $E_\gamma = 3.21$ MeV peak of interest. The events of interest are those which are within either (or both) of the aforementioned red and blue dashed regions, with the projected spectra shown in panels (c)–(f) for the different time loci. The y-axis on the right side shows the normalized counts, accounting for the number of loci for each spectrum. The fit was performed with maximum likelihood estimation due to the very low statistics of the various background components.

finite-angle effects of the LaBr₃(Ce) detectors, the total response of the apparatus was simulated to produce energy-dependent, discrete values for the Legendre polynomials for each LaBr₃(Ce) detector of OSCAR. For all discrete fits, the systematic uncertainty from the geometry of OSCAR was accounted for by repeating the simulations and fits with the LaBr₃(Ce) detectors positioned at ± 1 mm from their nominal 16.3 cm displacement from the target. These resultant correction factors are summarized in Table III. The $E_\gamma = 3.214$ MeV efficiency ($\epsilon_{3.21}$) for γ decay from the Hoyle state was determined by using the $E_\gamma = 3.201$ MeV $0_2^+ \rightarrow 2_1^+$ transition in ^{28}Si as a proxy, corresponding to $\epsilon_{3.20}$. This approximation is justified as GEANT4 simulations demonstrate that $\epsilon_{3.21} \approx \epsilon_{3.20} \approx 0.101$. For the cases of ^{28}Si exclusively, a dataset with a proton beam energy of $E_p = 16.0$ MeV was employed. A measurement utilising SiO₂ was also performed in 2019, but the 0_2^+ in ^{28}Si was inaccessible. It was also done to avoid contamination of the 0_2^+ state in ^{28}Si with the $E_x = 3.68$ MeV and 3.85 MeV states from ^{13}C in the backing foil. By gating on the 0_2^+ state in ^{28}Si , the associated $E_\gamma = 3.201$ MeV γ -ray decay is isotropic. The corresponding efficiency required a relative 3% correction as the subsequent $2_1^+ \rightarrow 0_1^+$ γ -ray decay may interact with the detectors. The experimental value of $\epsilon_{3.20} = 0.101(4)$ agrees well with the simulated value of 0.101. The $E_\gamma = 4.439$ MeV efficiency ($\epsilon_{4.44}$) for γ decay from the 2_1^+ state was determined by gating on 2_1^+ events detected with SiRi (see Fig. 1). The anisotropy of this $E2$ γ -ray was fitted to determine the (relative 1%) angular-correlation correction factor to yield $\epsilon_{4.44} = 0.0833(13)$, which also agrees extremely well with the simulated value of 0.0832. The reason why both the data and fits of the angular correlations (relative to the beam direction) in Figs. 9(a) and 9(b) are slightly asymmetric across $\theta = 90^\circ$ is the increased attenuation from SiRi, which was configured at backward angles. To determine the $W_{020}^{7.65}$ angular-correction factor, the γ - γ angular correlations for the $0_2^+ \rightarrow 2_1^+ \rightarrow 0_1^+$ transitions in both ^{28}Si and ^{12}C were analyzed, see Figs. 9(c) and 9(d). These associated fits were of the form $W(\theta) = a_0 [1.0 + A_2 P_2(\cos \theta) + A_4 P_4(\cos \theta)]$, where $A_2 = 0.3571$ and $A_4 = 1.1429$ are theoretical coefficients and a_0 is the only free parameter in the fit [19]. These fits yielded $\chi_{\text{red}}^2 = 0.34$ and 0.74 for ^{28}Si and ^{12}C , respectively. Using these theoretical coefficients, the corresponding angular-correlation correction factors for the ^{28}Si and ^{12}C cases were both simulated to be $W_{020}^{7.65} = 0.96(2)$. The associated uncertainty is conservatively estimated by taking a weighted average of the relative uncertainty for each discretely fitted point in Fig. 9(c). This was then added in quadrature to that originating from the aforementioned ± 1 mm geometrical uncertainty. The use of the simulated $W_{020}^{7.65}$ value in Eq. 3 is justified as the corresponding theoretical (simulated) angular correlations describe the data appropriately.

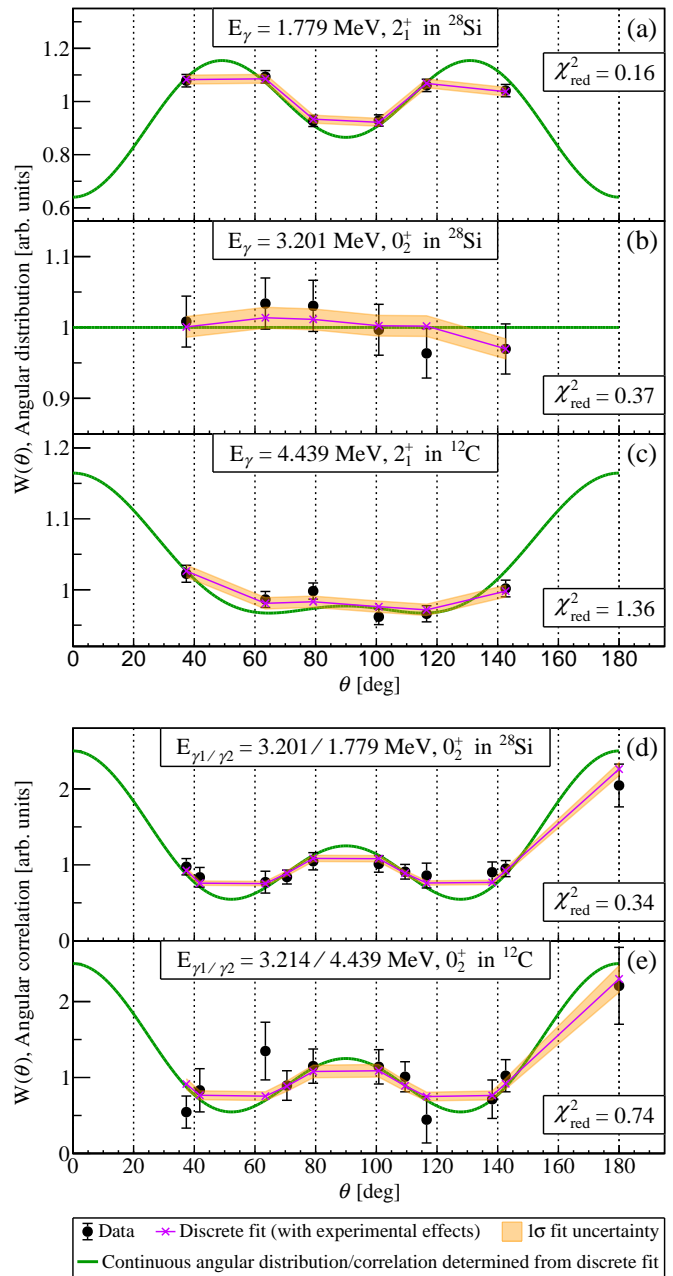


FIG. 9. Panels (a) and (b) present angular correlations between the γ ray and the beam direction. Panels (c) and (d) present γ - γ angular correlations between the pair of γ rays.

IV. RESULTS

For the measurements performed in 2019 and 2020, the extracted efficiencies and angular-correlation correction factors are summarized in Table III. For the extracted efficiencies of the CACTUS array (used in the 2014 measurement) see Appendix A 3. The associated results for all of these measurements (2014, 2019 and 2020) are summarized in Table II.

TABLE II. A summary of the inclusive and p - γ - γ triple-coincidence yields employed in Eq. 3 to determine Γ_γ/Γ , Γ_{rad}/Γ and Γ_{rad} . N_{020} represents the background-subtracted triple-coincidence yield. These reported uncertainties combine both statistical and systematic components.

	$^{12}\text{C}(p, p')$ with $E_p = 10.7$ MeV performed in 2014 [13]		$^{12}\text{C}(p, p')$ with $E_p = 10.8$ MeV performed in 2019		$^{28}\text{Si}(p, p')$ with $E_p = 16.0$ MeV performed in 2020	
	0_2^+ in ^{12}C using $\Sigma\gamma$	0_2^+ in ^{12}C using γ - γ	0_2^+ in ^{12}C using $\Sigma\gamma$	0_2^+ in ^{12}C using γ - γ	0_2^+ in ^{28}Si using $\Sigma\gamma$	0_2^+ in ^{28}Si using γ - γ
N_{inc}	$2.95783(4) \times 10^8$		$3.1922(4) \times 10^8$		$1.658(9) \times 10^5$	
N_{020}	223(27)	225(26)	1009(82)	1011(64)	2351(75)	2199(68)
N_{pr-pr}	223(26)	225(25)	1253(50)	1277(58)	2372(69)	2206(68)
N_{pr-dl}	$\approx 0(7)$	$\approx 0(7)$	271(23)	290(14)	21(2)	7(2)
N_{dl-dl}	$\approx 0(4)$	$\approx 0(4)$	24(7)	42(6)	$\approx 0(10)$	$\approx 0(3)$
$N_{dl-dl'}$	$\approx 0(4)$	$\approx 0(4)$	52(10)	67(4)	$\approx 0(1)$	$\approx 0.0(3)$
N_{020}/N_{inc}	$7.6(9) \times 10^{-7}$	$7.5(9) \times 10^{-7}$	$3.2(2) \times 10^{-6}$	$3.2(2) \times 10^{-6}$	$1.42(4) \times 10^{-2}$	$1.33(4) \times 10^{-2}$
Γ_γ/Γ	$6.6(8) \times 10^{-4}$	$6.6(8) \times 10^{-4}$	$4.0(4) \times 10^{-4}$	$4.0(3) \times 10^{-4}$	1.08(6)	1.01(5)
Γ_{rad}/Γ	$6.6(9) \times 10^{-4}$	$6.7(9) \times 10^{-4}$	$4.1(4) \times 10^{-4}$	$4.1(4) \times 10^{-4}$		
Γ_{rad} [meV]	5.4(8)	5.4(8)	3.3(4)	3.4(4)		

TABLE III. The experimental and simulated correction factors employed in Eq. 3 and Eq. A1 for OSCAR. The absolute photopeak efficiencies account for any required corrections, such as scattering/summing effects and/or anisotropic angular distributions. These efficiencies are presented as fractions, per detector.

	$^{12}\text{C}(p, p')$ with $E_p = 10.8$ MeV performed in 2019		$^{28}\text{Si}(p, p')$ with $E_p = 16.0$ MeV performed in 2020	
	$\epsilon_{1.78}$ (simulation)			0.00457(3)
$\epsilon_{1.78}$ (measured)			$0.00479(4)_{stat.} \times 0.98(2)_{syst.} = 0.0047(1)$	
$\epsilon_{3.20}$ (simulation)			0.00337(3)	
$\epsilon_{3.20}$ (measured)			$0.00326(5)_{stat.} \times 1.03(2)_{syst.} = 0.00336(9)$	
$\epsilon_{3.21}$ (simulation)		0.00337(3)		
$\epsilon_{3.21}$ (measured)				
$\epsilon_{4.44}$ (simulation)		0.00277(3)		
$\epsilon_{4.44}$ (measured)		$0.002747(5)_{stat.} \times 1.01(2)_{syst.} = 0.00278(4)$		
$W_{020}^{E_\gamma}$ (simulation)		0.96(2)		0.96(2)
$W_{020}^{E_\gamma}$ (measured)				0.96(4)

A. $^{12}\text{C}(p, p')$ with $E_p = 10.8$ MeV performed in 2019

The γ -decay branching ratio of the Hoyle state was determined with Eq. 3 and the values reported in Table II and III to be $\Gamma_\gamma^{E2}/\Gamma = 4.0(3) \times 10^{-4}$ when using the triple-coincidence yields obtained through γ - γ , and $\Gamma_\gamma^{E2}/\Gamma = 4.0(4) \times 10^{-4}$ when using the triple-coincidence yields obtained through summed- γ matrices. In this work, the latter value is used to calculate the associated radiative branching ratio and radiative width in order to implement a more conservative uncertainty. Using the theoretical total conversion coefficient, $\alpha_{tot}(E2, E_\gamma = 3.21 \text{ MeV}) = 8.77(13) \times 10^{-4}$ [13, 20] and

the recommended value of $\Gamma_\pi(E0)/\Gamma = 7.6(4) \times 10^{-6}$ from Eriksen *et al.* [21], the radiative branching ratio of the Hoyle state was determined as $\Gamma_{rad}/\Gamma = 4.1(4) \times 10^{-4}$ for both methods of triple-coincidence yield extraction. Using Eq. 1, the radiative width of the Hoyle state is determined as $\Gamma_{rad} = 3.4(4)$ meV in this work.

B. $^{28}\text{Si}(p, p')$ with $E_p = 16.0$ MeV performed in 2020

The γ -decay branching ratio of the 4.98 MeV 0_2^+ state in ^{28}Si was determined with Eq. 3 and the values reported

in Table II and III to be $\Gamma_\gamma^{E2}/\Gamma = 1.01(5)$ when using the triple-coincidence yields obtained through γ - γ , and $\Gamma_\gamma^{E2}/\Gamma = 1.08(6)$ when using the triple-coincidence yields obtained through summed- γ matrices.

C. $^{12}\text{C}(p, p')$ with $E_p = 10.7$ MeV performed in 2014

In order to understand the discrepancy between the results of this work and Ref. [13], the analysis methodology used in this work was employed to independently verify aspects of the analysis in Ref. [13]. In this work, the inclusive and triple-coincidence yields for the 2014 experiment of Ref. [13] were determined, see Table II. The CACTUS efficiencies employed in this work were independently extracted from the same 2014 measurement, as well as from two measurements performed in 2012 (see Table VII for a summary). The efficiency at $E_\gamma = 4.44$ MeV was determined by an uncertainty weighted average of the values presented in Table VII to be $\epsilon_{4.44} = 0.00131(3)$ for a single detector in CACTUS. Both inclusive and triple-coincidence yields from this independent analysis are $\approx 5\%$ larger than the values of $N_{\text{inc}} = 2.78(6) \times 10^8$ and $N_{020}^{7.65} = 217(21)$ reported in Ref. [13] (yields presented in Table II). This difference is mostly due to different gates and/or fit methods. However, there is good agreement between the ratio of $N_{020}^{7.65}/N_{\text{inc}}^{7.65} = 7.8(9) \times 10^{-7}$ from Ref. [13] and the ratios in Table II obtained from the independent analysis of the 2014 experiment in this work. The independently determined yields in this work validate the corresponding yield-extraction methods performed in Ref. [13].

For the absolute full-energy photopeak efficiencies and detector combinations in Eq. 3, a significant discrepancy was determined between this work and the study by Kibédi *et al.* [13]. Firstly, γ -ray photopeak efficiencies reported in Ref. [13] are not absolute as was reported, but relative. Notably, the CACTUS efficiencies in Ref. [13] were determined from simulation, whereas all γ -ray efficiencies reported in this work were determined through experimental data. Secondly, the number of detector combinations (c_{det}) in Ref. [13] was incorrectly reported as $c_{\text{det}} = n_{\text{det}}(n_{\text{det}} - 1)/2 = 325$, whereas the correct value is $c_{\text{det}} = n_{\text{det}}(n_{\text{det}} - 1) = 650$. This c_{det} factor was not explicitly defined in Eq. 2 of Ref. [13], which is analogous to Eqs. 3 and A1 in this work. Due to these findings, the γ -decay branching ratio determined with Eq. 2 in Ref. [13] should be disregarded from future evaluations. However, the γ -decay branching ratio determined with Eq. 3 in Ref. [13] is still valid as this equation only requires relative efficiencies and does not depend on c_{det} . Thus, the main result of $\Gamma_{\text{rad}}/\Gamma = 6.2(6) \times 10^{-4}$ reported in Ref. [13] remains valid. In the independent reanalysis of the 2014 experiment in this work, the radiative branching ratio of the Hoyle state was determined to be $\Gamma_{\text{rad}}/\Gamma = 6.6(9) \times 10^{-4}$ and $\Gamma_{\text{rad}}/\Gamma = 6.7(9) \times 10^{-4}$ (using the γ - γ and summed-

γ matrices, respectively), which are in agreement with the result reported by Kibédi *et al.* [13].

V. DISCUSSION

A summary of previous results for the radiative branching of the Hoyle state in ^{12}C is presented in Table IV. The radiative branching ratio reported in this work of $\Gamma_{\text{rad}}/\Gamma = 4.1(4) \times 10^{-4}$ for the Hoyle state (from the 2019 measurement, see Table II) agrees well with the adopted value of $\Gamma_{\text{rad}}/\Gamma = 4.16(11) \times 10^{-4}$ given by Kelley *et al.* [4] as well as all recent measurements, with the lone exception being the result by Kibédi *et al.* [13], which is significantly larger. To investigate the discrepantly large result by Kibédi *et al.* [13], the analysis methodology used in this work was employed to independently verify aspects of the analysis in Ref. [13]. For the same 2014 measurement studied in Ref. [13], the independent analysis in this work yielded $\Gamma_{\text{rad}}/\Gamma = 6.7(9) \times 10^{-4}$, which is in excellent agreement with the result in Ref. [13]. Consequently, this work verifies the yield-extraction method employed in Ref. [13]. To verify the analysis method in this work, the $0_2^+ \rightarrow 2_1^+ \rightarrow 0_1^+$ cascade in ^{28}Si was employed as a surrogate for the analogous cascade for the Hoyle state. The advantage of this cascade is that the 0_2^+ state in ^{28}Si decays exclusively via γ decay, thus providing a large yield of γ decays with a reference value of $\Gamma_\gamma/\Gamma = 1$ [22]. For the 0_2^+ state in ^{28}Si , the analysis method in this work yielded $\Gamma_\gamma/\Gamma = 1.07(8)$ from the triple coincidences obtained through γ - γ and $\Gamma_\gamma/\Gamma = 1.09(7)$ for the triple coincidences obtained through summed- γ for the $^{28}\text{Si}(p, p')$ measurement in 2012. Similarly, this work reports $\Gamma_\gamma/\Gamma = 1.08(6)$ for triple coincidences obtained through summed- γ and $\Gamma_\gamma/\Gamma = 1.01(5)$ for triple coincidences obtained through γ - γ for the $^{28}\text{Si}(p, p')$ measurement in 2020. These results indicate that the analysis method employed in this work is valid. However, in principle, it is possible that there may have existed systematic errors in the experimental setup of the 2014 measurement [13] which only become apparent for rare decay channels which yield low signal-to-background ratios. Unfortunately, such possible systematic errors arising from the experimental setup employed in the 2014 experiment [13] cannot be investigated as that setup has been decommissioned. Therefore, the underlying cause for the discrepant result published in Ref. [13] could not be determined in this work.

A physical justification for the discrepant γ -decay branching ratio reported in Ref. [13] was suggested by Cardella *et al.* [11, 24] as originating from the hypothetical Efimov state in ^{12}C . If the Efimov state manifests at the predicted energy of $E_x = 7.485$ MeV [25], then such a contamination to the result by Kibédi *et al.* [13] and the corresponding reanalysis in this work can be excluded. Firstly, the photopeak of the $E_\gamma = 3.018$ MeV $E2$ γ decay from the Efimov state would be clearly re-

TABLE IV. Summarised results of recent measurements for the radiative branching ratio of the Hoyle state.

Reference	$\Gamma_{\text{rad}}/\Gamma \times 10^4$	Methodology
Kelley [4]	4.16(11)	Adopted value
Kibédi [13]	6.2(6)	γ -ray spectroscopy
Tsumura [10]	4.3(8)	Charged-particle spectroscopy
Luo [23]	4.0(3)	Charged-particle spectroscopy
This work	4.1(4)	γ -ray spectroscopy

solved from the $E_\gamma = 3.214$ MeV photopeak in Fig. 7(c). Secondly, the ejectiles corresponding to the Hoyle and Efimov states would be separated by 150 or 250 keV, corresponding to a 0 or 25 μm deadlayer in SiRi, respectively (a 25 μm deadlayer is required to reproduce the ordering of the peaks in Figs. 1 and 5). If the Efimov state was sufficiently populated at exactly $E_x = 7.485$ MeV, the ≈ 90 keV FWHM resolution of the ΔE detectors in SiRi would enable such a contamination to be observable. Fig. 10 presents a selective test for such a contamination in the ΔE spectrum by gating on the $E_\gamma = 3.21$ MeV and $E_\gamma = 4.44$ MeV γ -ray photopeaks from the Hoyle state (with the same background subtraction method as applied in Sec. III B). If the dis-

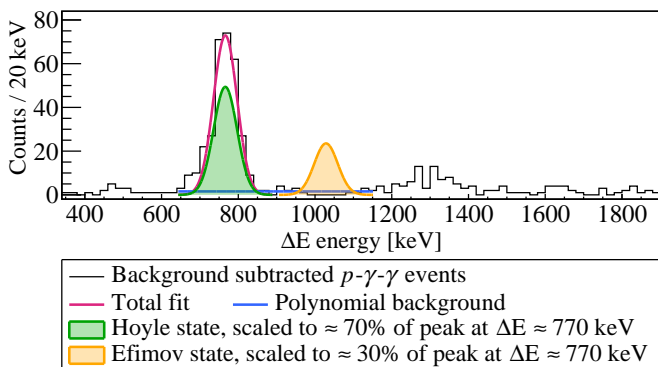


FIG. 10. ΔE spectrum for the 2014 $^{12}\text{C}(p, p')$ measurement, gated on the $E_\gamma = 3.21$ MeV and $E_\gamma = 4.44$ MeV γ -ray photopeaks from the Hoyle state (see text for details).

crepancy between the γ -decay branching ratio reported by Ref. [13] ($\Gamma_\gamma^{E2}/\Gamma = 6.1(6) \times 10^{-4}$) and the ENSDF average ($\Gamma_{\text{rad}}/\Gamma = 4.16(11) \times 10^{-4}$) [4] is assumed to be purely due to the Efimov state, the corresponding Efimov contribution would be $\approx 30\%$ of the triple-coincidence yield reported by Kibédi *et al.* [13] and in the independent analysis of the 2014 data performed in this work (see Table II). Such a division of the triple-coincidence yield is completely excluded by the data as no such peak is observed at $\Delta E \approx 1.030$ MeV (corresponding to $E_x = 7.485$ MeV). Furthermore, a possible contaminant Efimov state should affect the results of both the 2014 and 2019 experiments since these experimental conditions were very similar in both beam energy and detector configurations. However, only the 2014 measurement (Ref. [13] and the

independent reanalysis in this work) yields a discrepantly large γ -decay branching ratio for the Hoyle state (see Table II). Finally, a study by Bishop *et al.*, which employed the β -decay population of ^{12}C states and astrophysical-rate calculations, has yielded strong evidence *against* the very existence of the Efimov state at $E_x = 7.485$ MeV in ^{12}C [26]. From these arguments, we conclude that contamination from the hypothetical Efimov state is unlikely to explain why the radiative branching ratio of the Hoyle state reported by Ref. [13] is discrepant.

VI. CONCLUSION

In summary, a new measurement of the γ -decay and radiative branching ratio of the Hoyle state has been performed using OSCAR at the OCL. In this work, the reported radiative branching ratio of $\Gamma_{\text{rad}}/\Gamma = 4.1(4) \times 10^{-4}$ is in good agreement with the previously adopted value of $\Gamma_{\text{rad}}/\Gamma = 4.19(11) \times 10^{-4}$ from Kelley *et al.* [4] as well as recent measurements by Luo *et al.* [23] and Tsumura *et al.* [10]. The analysis method employed in this study was verified with the extraction of the radiative branching ratio of the 0_2^+ state in ^{28}Si at $E_x = 4.98$ MeV.

In this work, it was determined that the γ -ray photopeak efficiencies reported in Ref. [13] are not absolute as was reported, but relative. Furthermore, the number of detector combinations employed in Ref. [13] was incorrect. However, the main result of Ref. [13] was determined to still be valid as two methods were employed in Ref. [13] to calculate the γ -decay branching ratio of the Hoyle state. One of these methods only required relative efficiencies and did not depend on the detector combinatorics. In this work, an independent reanalysis was performed on the 2014 measurement reported by Kibédi *et al.* [13] and the obtained radiative branching ratio of the Hoyle state was in good agreement with Ref. [13]. Therefore, the underlying cause for the discrepant result published in Ref. [13] could not be determined in this work.

More independent, innovative measurements for the radiative width of the Hoyle state are crucial, as this quantity directly determines the astrophysically significant triple- α reaction rate. Such new measurements will further substantiate whether the discrepant result by Kibédi *et al.* [13] should be excluded from future evaluations.

ACKNOWLEDGMENTS

This study has been funded by the Research Council of Norway through its grant to the Norwegian Nuclear Research Centre (Project No. 341985, 245882 and 325714). The authors would like to thank J. C. Müller, P. A. Sobas, and J. C. Wikne at the Oslo Cyclotron Laboratory (OCL) for the accelerated proton beams. We would like to thank

F. Zeiser for his contributions through the development of the GEANT4 simulation. The computations were performed on resources provided by UNINETT Sigma2 - the National Infrastructure for High Performance Computing and Data Storage in Norway (using “SAGA” on Project No. NN9895K and NN9464K). A. C. Larsen gratefully acknowledges funding of this research by the European Research Council through ERC-STG-2014 under Grant Agreement No. 637686 and from the Research Council of Norway, Project Grant No. 316116.

Appendix A: Appendix

1. Analysis method for $^{28}\text{Si}(p, p')$ measurement with $E_p = 16.0$ MeV performed in 2020

The primary objectives of the analysis of the data from 2020 are to test the validity of the analysis method employed in Sec. III A and to obtain efficiencies for the LaBr₃(Ce) detectors which comprise OSCAR. The 0_2^+ state at $E_x = 4.98$ MeV in ^{28}Si has a γ -decay branching ratio of $\Gamma_\gamma/\Gamma = 1$ and emits a γ ray with $E_\gamma = 3.20$ MeV. This transition is followed by a $E_\gamma = 1.79$ MeV γ ray from the 2_1^+ $E_x = 1.79$ MeV state to the ground state in ^{28}Si . The reason why the γ -ray cascade from the 0_2^+ state in ^{28}Si is a good surrogate for that of the Hoyle state is because the spin and parities of the corresponding states are the same. This results in an identical angular correlation for the cascade. In addition, the $E_\gamma = 3.20$ ($0_2^+ \rightarrow 2_1^+$) transition is almost identical in energy to the γ ray emitted from the Hoyle state. Finally, since $\Gamma_\gamma/\Gamma = 1$ for the 0_2^+ in ^{28}Si , the branching ratio for this state can be calculated as a validation of the overall analysis method. The $\Gamma_\gamma^{E_2}/\Gamma$ branching ratio of the 0_2^+ state at $E_x = 4.98$ MeV in ^{28}Si can be expressed as

$$\frac{\Gamma_\gamma^{4.98}}{\Gamma} = \frac{N_{020}^{4.98}}{N_{\text{inclusive}}^{4.98} \times \epsilon_{1.78} \times \epsilon_{3.20} \times c_{\text{det}} \times W_{020}^{4.98}} = 1.0, \quad (\text{A1})$$

which is analogous to Eq. 3.

For the $^{28}\text{Si}(p, p')$ reaction with a beam energy $E_p = 16.0$ MeV performed in 2020, both layers of SiRi could be used. The energy depositions in SiRi are shown in Fig. 11 (a), and the sum of the relevant ΔE -E energies are shown in Fig. 11 (b), with the violet colored area denoting the energy gate around the 0_2^+ state at $E_x = 4.98$ MeV in ^{28}Si . Due to the kinematic smearing, the data from each ring are fitted separately. Fig. 12 shows the time difference between detected proton ejectiles corresponding to the Hoyle state, and the LaBr₃(Ce) timing signals corresponding to the γ -ray cascade from the 0_2^+ state at $E_x = 4.98$ MeV. As the total statistics is much lower in this experiment compared to the other experiments (2019 and 2014, see Sec. III A and Sec. III B) combined with the much cleaner signal, the total yield in the timing matrix is also lower.

In Fig. 13(a) the γ - γ matrix gated on the pr-pr time

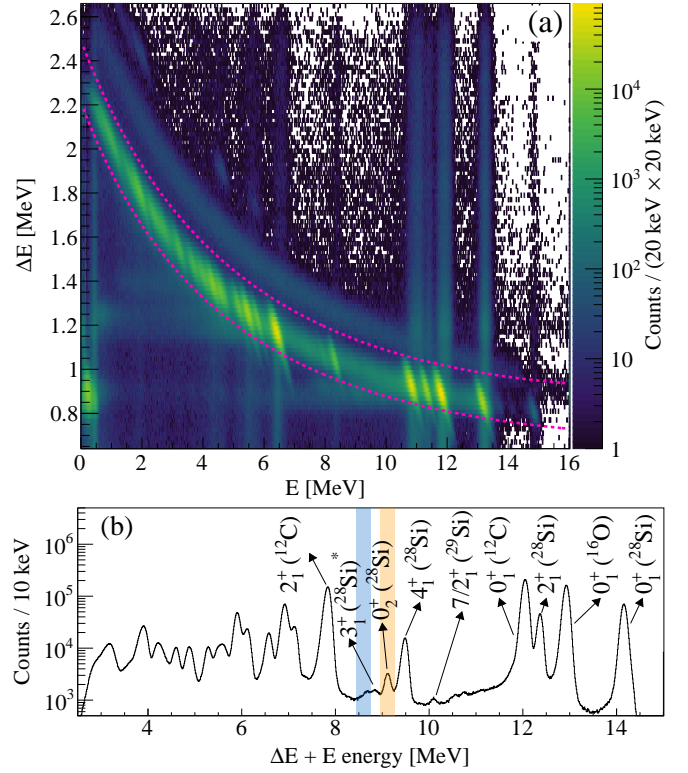


FIG. 11. (a) ΔE - E energy spectrum of ejectiles, detected at $\theta_{\text{lab}} = 128^\circ$ – 130° with SiRi from the measurement performed in 2020. The violet lines denote the energy gate employed for the inelastically scattered protons. (b) The sum of ΔE - E events in the violet gated area in (a). The orange filled area at $E_p \approx 9$ MeV denotes the energy gate employed for the 0_2^+ state in ^{28}Si . The state denoted $3_1^+ (^{28}\text{Si})^*$ also has γ -ray transitions consistent with states from ^{29}Si and ^{30}Si . The blue shaded area denotes the energy gate employed for the background gated analysis, as explained in Appendix A 2.

locus is shown. The red, dashed horizontal lines correspond to the 3σ gate employed on the $E_\gamma = 1.78$ MeV γ -ray in the 0_2^+ cascade at $E_x = 4.98$ MeV in ^{28}Si , with a zoomed-in region focused on the $E_\gamma = 1.78$ MeV and $E_\gamma = 3.20$ coincidence locus shown in Fig. 13(b). The γ -ray spectra corresponding to these gated γ - γ matrices (for the various time loci pr-pr, pr-dl, dl-dl and dl-dl'), the simultaneous fit is shown in Fig. 13(c)–(f). Due to the very clean signal in this experiment and the low statistics of the background components, a fit using maximum likelihood estimation was performed.

The summed- γ matrix gated on the pr-pr time locus is presented on Fig. 14(a). By gating on such summed- γ matrices for different timing loci, the corresponding triple-coincidence yields can be extracted. Fig. 14(c)–(f) presents the simultaneous fit of these spectra, which was performed with maximum likelihood estimation due to the very low statistics of the various background components. The yields from the $N_{\text{pr-dl}}$, $N_{\text{dl-dl}}$ and $N_{\text{dl-dl}'}$ background components are negligible for both methods of extraction. The uncertainties of weakly popu-

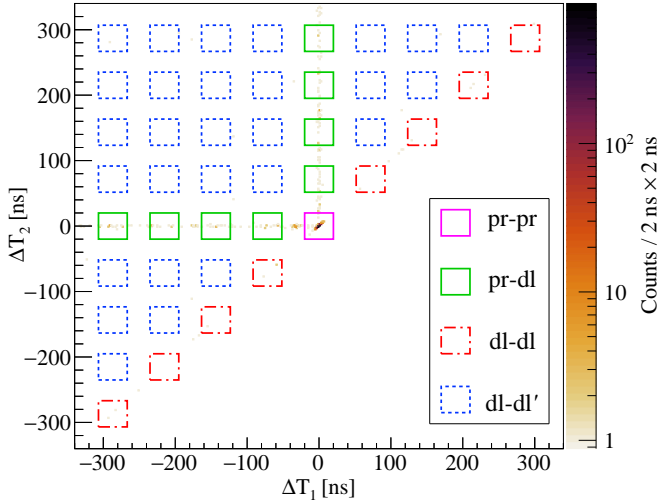


FIG. 12. Time differences between protons populating the 0_2^+ state at $E_x = 4.98$ MeV in ^{28}Si and two γ rays with $E_\gamma = 3.20$ MeV and $E_\gamma = 1.79$ MeV, from the experiment performed in 2020. The matrix is sorted so the largest value of the two timing values is along the y-axis. The colored boxes denote the different background gates used for the analysis.

lated peaks were conservatively estimated by adding (in quadrature) the statistical uncertainty of the histogram in the range of the peak.

2. Investigation of background in inclusive particle spectra

For each measurement presented in Table I, the nature of the background events beneath the inclusive peak of interest (in SiRi) was investigated. Three cases comparing the effect on the triple-coincidence yields are each presented in Figs. 15 and 16. The first case corresponding to a gate on the inclusive peak of interest and the pr-pr time locus. The second case corresponding to a gate on the inclusive peak of interest with background subtraction according to Eq. 4. The third case corresponds to a gate on the smooth region close to the inclusive peak of interest, with background subtraction according to Eq. 4. In some cases, these background gates were of a different size than for the peak of interest and for such cases, the scaling of the corresponding triple-coincidence spectra was commensurate.

Good selectivity with SiRi was observed as the correlated γ -ray peaks are negligible for the background-regions in the inclusive spectra. However, several uncorrelated peaks persist even after background subtraction by gating on different time loci. The relative strength of these uncorrelated γ -ray peaks are reproduced in the triple-coincidence spectra gated on the smooth region near the peak of interest. This indicates that the uncorrelated γ -ray peaks which persist through timing-related background subtraction (in Figs. 3, 4, 7 and 8) are due to

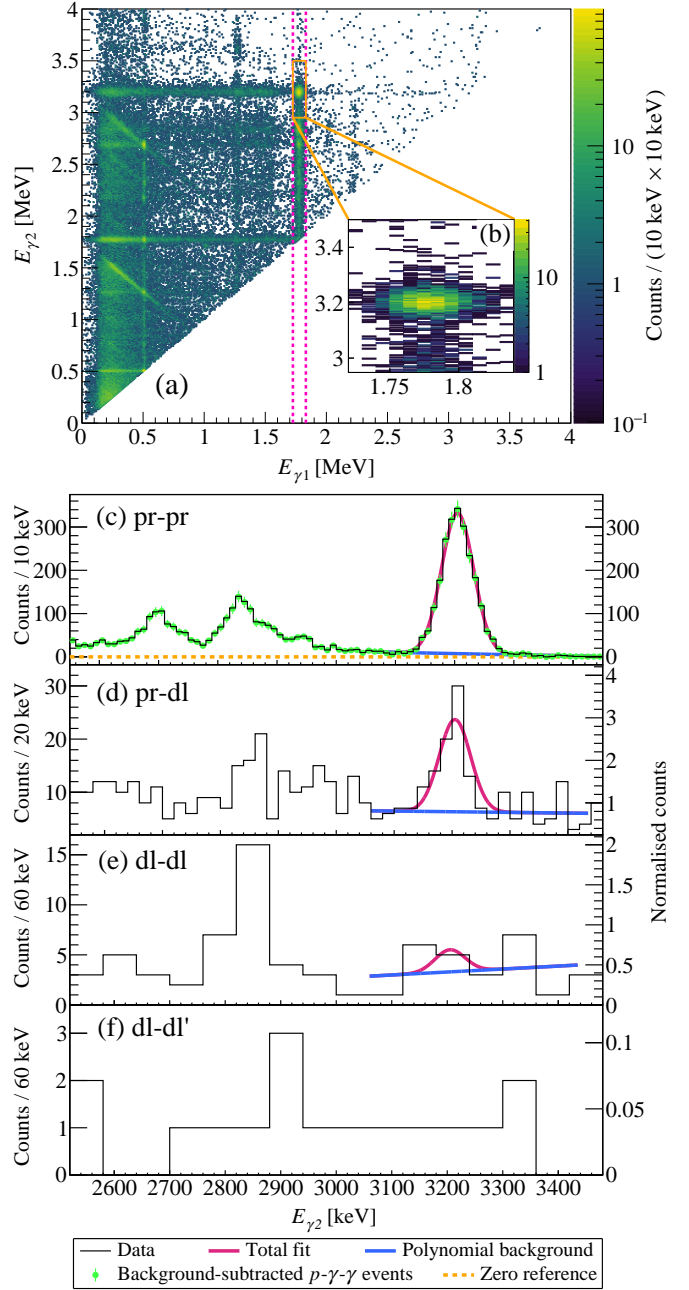


FIG. 13. (a) The γ - γ matrix (largest energy on the y-axis) gated on the pr-pr time locus (see Fig. 12) from $^{28}\text{Si}(p, p')$ measurement performed in 2020. A zoomed-in region, indicated with solid violet lines, is shown in panel (b). The horizontal, red dashed lines correspond to the 3σ gate on the summed- γ energies from the 0_2^+ state at $E_x = 4.98$ MeV in ^{28}Si . The events of interest are those within the aforementioned red dashed region, with the projected spectra shown in panels (c)–(f) for the different time loci. The y-axis on the right side shows the normalized counts, accounting for the number of loci for each spectrum. This simultaneous fit was performed with maximum likelihood estimation due to the very low statistics of the various background components.

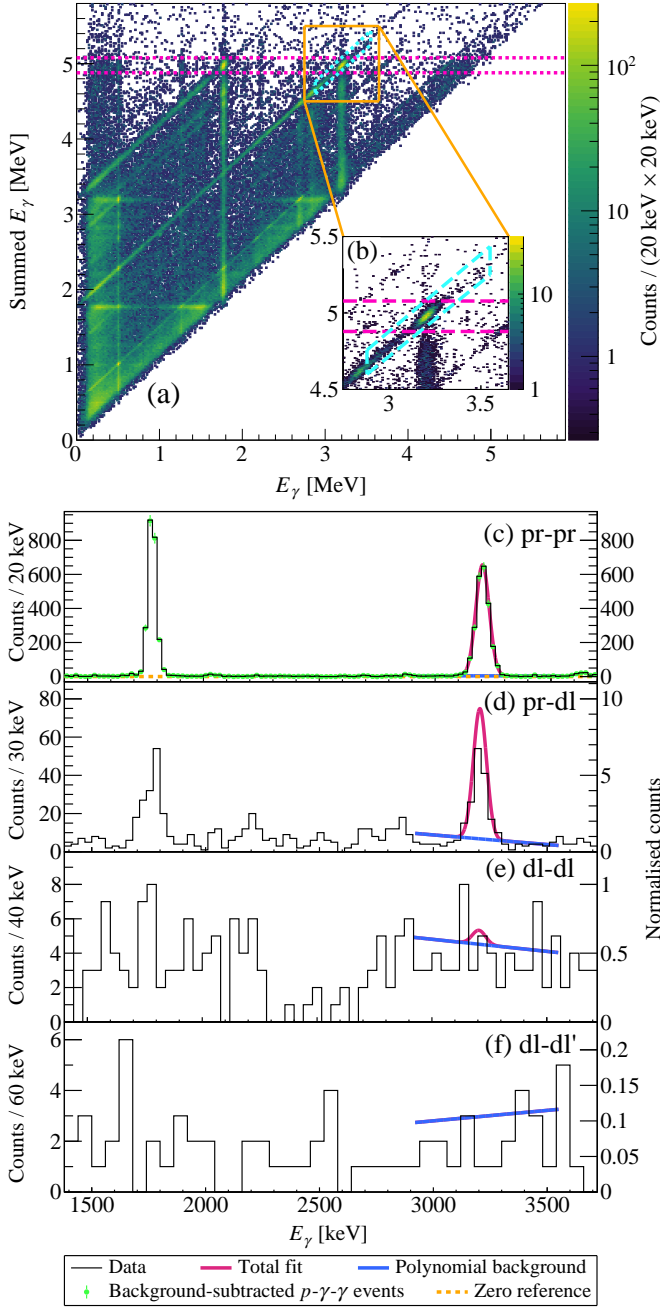


FIG. 14. (a) The summed- γ matrix gated on the pr-pr time locus (see Fig. 12) from $^{28}\text{Si}(p, p')$ measurement performed in 2020. A zoomed-in region, indicated with solid violet lines, is shown in panel (b). The horizontal, red dashed lines correspond to the 3σ gate on the summed- γ energies from the 0_2^+ state at $E_x = 4.98$ MeV in ^{28}Si . The lower region in the blue dashed lines corresponds to the smooth Compton continuum from the $E_\gamma = 3.20$ MeV peak of interest. The events of interest are those which are within either (or both) of the aforementioned red and blue dashed regions, with the projected spectra shown in panels (c)–(f) for the different time loci. The y-axis on the right side shows the normalized counts, accounting for the number of loci for each spectrum. This simultaneous fit was performed with maximum likelihood estimation due to the very low statistics of the various background components.

TABLE V. Summary of the labeled features in Fig. 15.

Label	Energy [keV]	Source
(1)	511	
(2)	844	^{27}Al
(3)	1015	^{27}Al
(4)	2212	^{27}Al
(5)	3214	^{12}C
(6)	3927	First-escape of 4440 keV in ^{12}C
(7)	4440	^{12}C
(8)	511	
(9)	844	^{27}Al
(10)	1015	^{27}Al
(11)	1436	^{138}La
(12)	1720	^{27}Al
(13)	2212	^{27}Al
(14)	3004	^{27}Al
(15)	3214	^{12}C
(16)	3416	Second-escape of 4440 keV in ^{12}C
(17)	3927	First-escape of 4440 keV in ^{12}C
(18)	4440	^{12}C
(19)	2713	^{29}Si
(20)	2838	^{28}Si
(21)	3201	^{28}Si

scattered ejectiles which lie beneath the inclusive peak of interest. Tables V and VI summarize the various transitions in Figs. 15 and 16.

3. Efficiency of CACTUS

The CACTUS efficiency at $E_\gamma = 4.44$ MeV was obtained from the $^{12}\text{C}(p, p')$ reaction at the $E_x = 4.44$ MeV 0_1^+ state in ^{12}C from the measurement performed in 2014. For Eq. 3 and Eq. A1, additional efficiency points were derived from two measurements in 2012. One of these measurements also provided a second efficiency point at $E_\gamma = 4.44$ MeV from the $E_x = 4.44$ MeV 0_1^+ state in ^{12}C . Experimental efficiency points at $E_\gamma = 1.78$ MeV and $E_\gamma = 3.20$ MeV were obtained from the $E_x = 1.78$ MeV 2_1^+ state and $E_x = 4.98$ MeV 0_2^+ state in ^{28}Si , respectively. These measurements were selected as they utilized a higher beam energy of 16.0 MeV, facilitating the use of both layers of SiRi for increased ejectile selectivity. Table VII provides the experimental details and measured efficiencies for all three measurements used to determine these efficiencies. A systematic uncertainty of

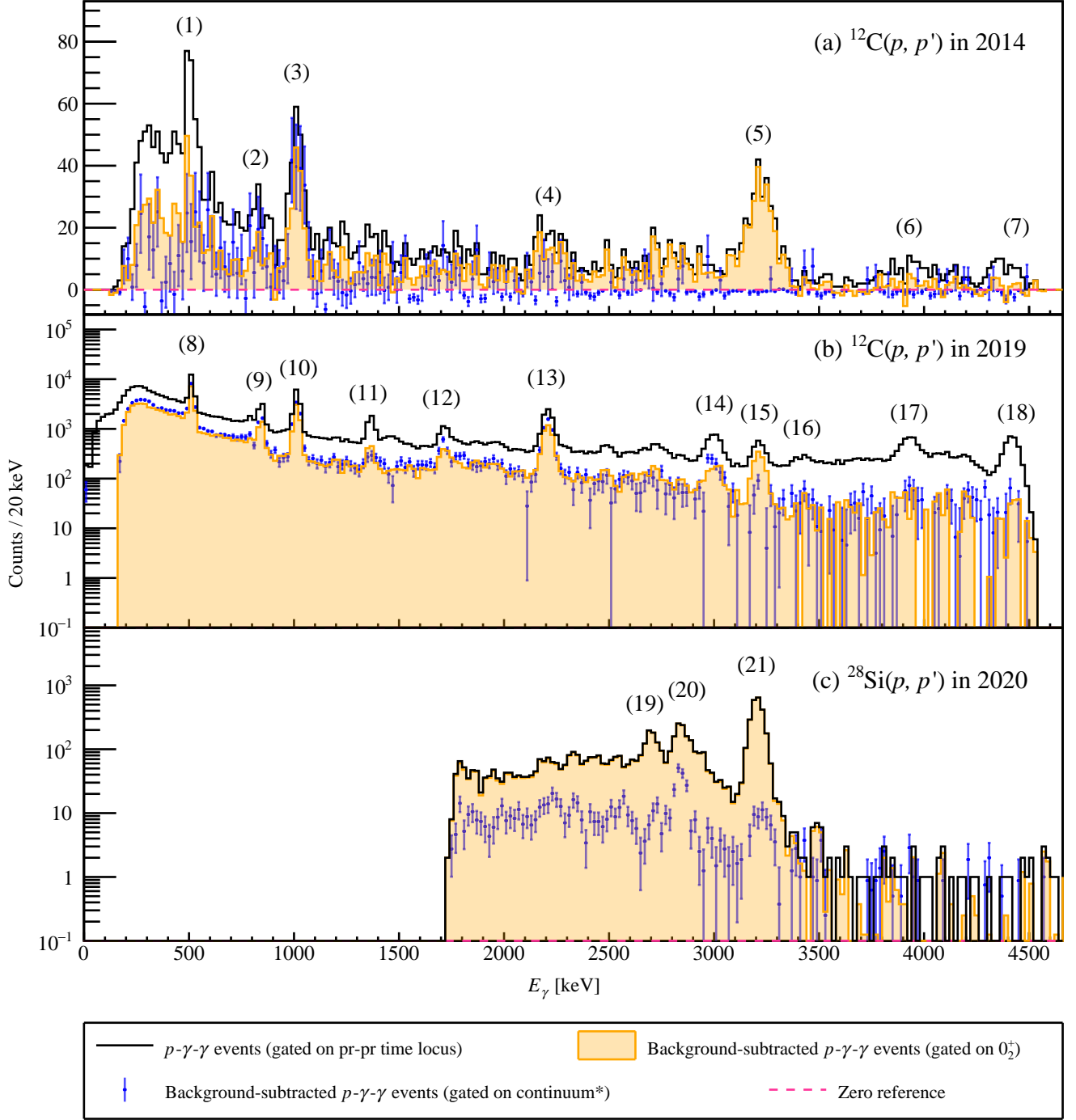


FIG. 15. A comparison of $p\text{-}\gamma\text{-}\gamma$ events obtained from the $\gamma\text{-}\gamma$ matrix with different conditions on the gating on the particle spectrum. Events gated on the 0_2^+ state in the nucleus of interest and the "pr-pr" time locus are indicated in black in all panels. By subtracting the background using Eq. 4, the background-subtracted $p\text{-}\gamma\text{-}\gamma$ events gated on the 0_2^+ state in the nucleus of interest are shown in purple. Additionally, the background-subtracted $p\text{-}\gamma\text{-}\gamma$ events when gating on the continuum in the nucleus of interest are illustrated in green in all panels. A pink horizontal dashed line shows the zero reference in all panels. Panel (a) shows the comparison for the $^{12}\text{C}(p, p')$ reaction populated in 2014 (see Sec. III B for more information). Panel (b) shows the comparison for the $^{12}\text{C}(p, p')$ reaction populated in 2019 (see Sec. III A for more information). Panel (c) shows the comparison for the $^{28}\text{Si}(p, p')$ reaction populated in 2020 (see Appendix A 1 for more information).

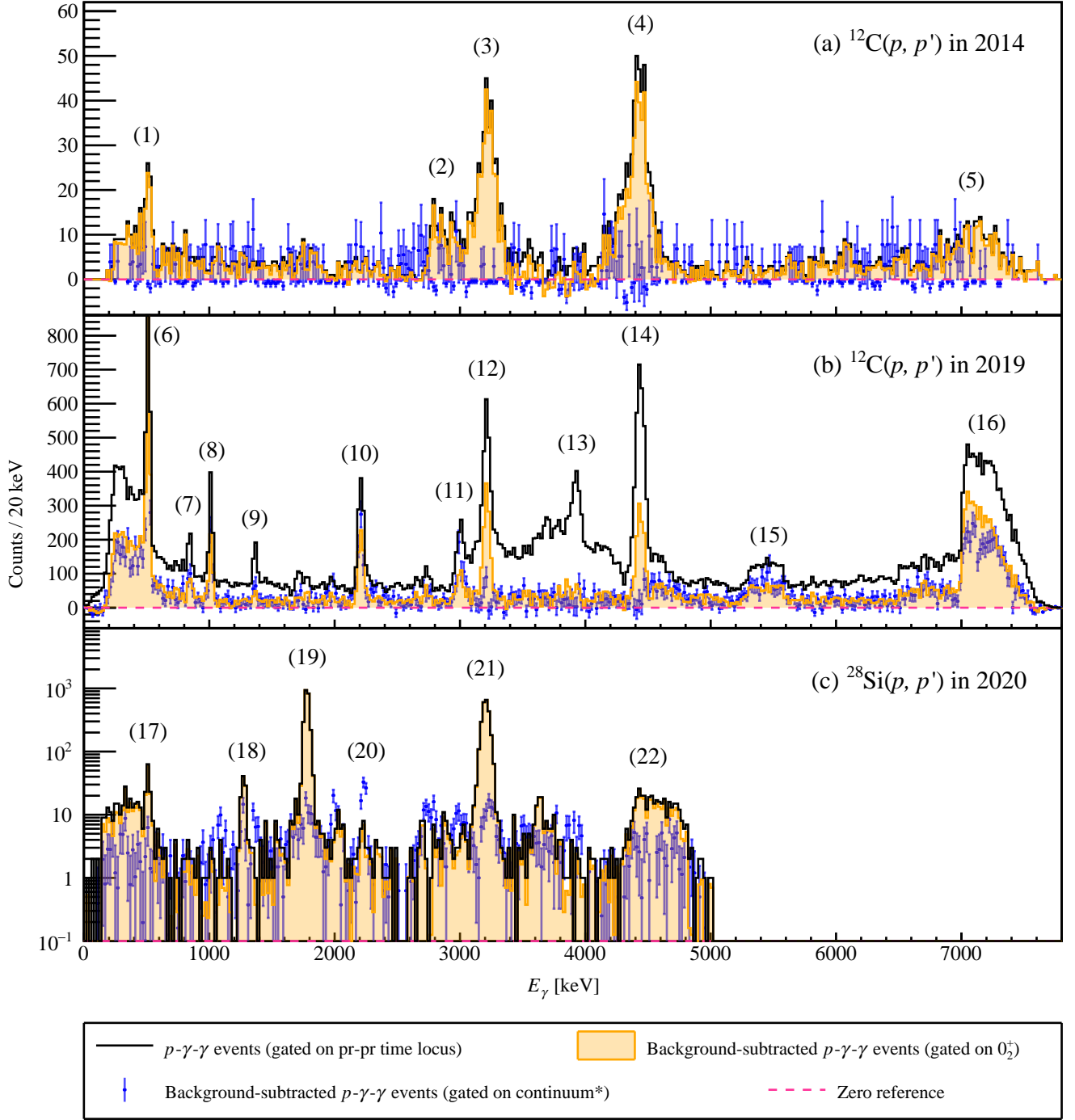


FIG. 16. A comparison of $p\text{-}\gamma\text{-}\gamma$ events obtained from the summed- γ matrix with different conditions on the gating on the particle spectrum. Events gated on the 0_2^+ state in the nucleus of interest and the "pr-pr" time locus are indicated in black in all panels. The gate on the summed- γ matrix in these spectra consists of only a 3σ band around the summed γ -ray energy of interest, in contrast to the modified gate used to extract $p\text{-}\gamma\text{-}\gamma$ events (see Sec. III A for more information). By subtracting the background using Eq. 4, the background-subtracted $p\text{-}\gamma\text{-}\gamma$ events gated on the 0_2^+ state in the nucleus of interest are shown in purple. Additionally, the background-subtracted $p\text{-}\gamma\text{-}\gamma$ events when gating on the continuum in the nucleus of interest are illustrated in green in all panels. A pink horizontal dashed line shows the zero reference in all panels. Panel (a) shows the comparison for the $^{12}\text{C}(p, p')$ reaction populated in 2014 (see Sec. III B for more information). Panel (b) shows the comparison for the $^{12}\text{C}(p, p')$ reaction populated in 2019 (see Sec. III A for more information). Panel (c) shows the comparison for the $^{28}\text{Si}(p, p')$ reaction populated in 2020 (see Appendix A 1 for more information).

TABLE VI. Summary of the labeled features in Fig. 16.

Label	Energy [keV]	Source
(1)	511	
(2)	≈ 2900	Compton scattered 3004 keV from ^{27}Al
(3)	3214	^{12}C
(4)	4440	^{12}C
(5)	≈ 7100	Compton scattered 4440 keV from ^{12}C
(6)	511	
(7)	844	^{27}Al
(8)	1015	^{27}Al
(9)	1436	^{138}La
(10)	2212	^{27}Al
(11)	3004	^{27}Al
(12)	3214	^{12}C
(13)	3927	First-escape of 4440 keV in ^{12}C
(14)	4440	^{12}C
(15)	≈ 5400	Compton background in coincidence with 2212 keV (10) from ^{27}Al
(16)	≈ 7200	Compton background in coincidence with low-energy below 511 keV (6)
(17)	511	
(18)	1273/1263	$^{29}\text{Si}/^{30}\text{Si}$
(19)	1779	^{28}Si
(20)	2212/2235	$^{27}\text{Al}/^{30}\text{Si}$
(21)	3201	^{28}Si
(22)	≈ 4500	Compton background in coincidence with low-energy below 511 keV (17)

3% was incorporated due to the absence of simulated correction factors for angular correlation and attenuation. In contrast, such corrections factors were employed for OSCAR, as discussed in Sec. III C.

4. Test of analysis method for CACTUS

In this work, the independent analysis of the 2014 $^{12}\text{C}(p, p')$ measurement (employing CACTUS) was validated by determining the well-known γ -decay branching ratio of the 0_2^+ state at $E_x = 4.98$ MeV in ^{28}Si . Details of this $^{28}\text{Si}(p, p')$ measurement are presented in column three of Table VII. This $^{28}\text{Si}(p, p')$ measured performed with $E_p = 16.0$ MeV enabled both layers of SiRi to be used for increased ejectile selectivity. Due to the lack of a GEANT4 simulation for the CACTUS array in this study, the angular correlation correction factor ($W_{020}^{4.98}$ from Eq. A1) presented in the work of Kibédi *et al.* [13] was used in this work. The use of $W_{020}^{4.98}$ from Ref. [13] does not play a significant role as this correction factor has been independently verified to be close to unity with OSCAR, which subtends similar angles to CACTUS. In this work, independent experimental efficiencies were used, as detailed in Appendix A3. The γ -decay branching ratio of the 0_2^+ state at $E_x = 4.98$ MeV in ^{28}Si was determined to be $\Gamma_\gamma/\Gamma = 1.07(8)$ when using the triple-coincidence yields obtained through γ - γ , and $\Gamma_\gamma/\Gamma = 1.09(7)$ when using the triple-coincidence yields obtained through summed- γ . These results thus validate the analysis method for the 2014 $^{12}\text{C}(p, p')$ measurement employing CACTUS.

-
- [1] E. M. Burbidge, G. R. Burbidge, W. A. Fowler, and F. Hoyle, Synthesis of the elements in stars, *Rev. Mod. Phys.* **29**, 547 (1957).
- [2] H. O. U. Fynbo, C. A. Diget, U. C. Bergmann, M. J. G. Borge, J. Cederkäll, P. Dendooven, L. M. Fraile, S. Franchoo, V. N. Fedosseev, B. R. Fulton, W. Huang, J. Huikari, H. B. Jeppesen, A. S. Jokinen, P. Jones, B. Jonson, U. Köster, K. Langanke, M. Meister, T. Nilsson, G. Nyman, Y. Prezado, K. Riisager, S. Rinta-Antila, O. Tengblad, M. Turrión, Y. Wang, L. Weissman, K. Wilhelmsen, J. Äystö, and T. I. Collaboration, Revised rates for the stellar triple-alpha process from measurement of ^{12}C nuclear resonances, *Nature* **433**, 136 (2005).
- [3] M. Freer and H. Fynbo, The Hoyle state in ^{12}C , *Progress in Particle and Nuclear Physics* **78**, 1 (2014).
- [4] J. Kelley, J. Purcell, and C. Sheu, Energy levels of light nuclei A=12, *Nuclear Physics A* **968**, 71 (2017).
- [5] F. Hoyle, D. N. F. Dunbar, W. A. Wenzel, and W. Whaling, A state in c-12 predicted from astrophysical evidence, in *Physical Review*, Vol. 92 (AMERICAN PHYSICAL SOC ONE PHYSICS ELLIPSE, COLLEGE PK, MD 20740-3844 USA, 1953) pp. 1095–1095.
- [6] D. N. F. Dunbar, R. E. Pixley, W. A. Wenzel, and W. Whaling, The 7.68-MeV state in C^{12} , *Phys. Rev.* **92**, 649 (1953).
- [7] M. Freer, H. Horiuchi, Y. Kanada-En'yo, D. Lee, and U.-G. Meißner, Microscopic clustering in light nuclei, *Rev. Mod. Phys.* **90**, 035004 (2018).
- [8] K. Li, F. Smit, P. Adsley, R. Neveling, P. Papka, E. Nikolskii, J. Brümmer, L. Donaldson, M. Freer, M. Harakeh, F. Nemulodi, L. Pellegri, V. Pesudo, M. Wiedeking, E. Buthelezi, V. Chudoba, S. Förtsch, P. Jones, M. Kamil, J. Mira, G. O'Neill, E. Sideras-Haddad, B. Singh, S. Siem, G. Steyn, J. Swartz, I. Usman, and J. van Zyl, Investigating the predicted breathing-mode

TABLE VII. A summary of the various experimental conditions used to determine the efficiency of the CACTUS array. The absolute photopeak efficiencies ($\epsilon_{1.78}$, $\epsilon_{3.20}$, $\epsilon_{4.44}$) are presented as fractions, per detector.

	$^{28}\text{Si}(p, p')$ with $E_p = 16.0$ MeV performed in 2012	$^{12}\text{C}(p, p')$ with $E_p = 16.0$ MeV performed in 2012	$^{12}\text{C}(p, p')$ with $E_p = 10.7$ MeV performed in 2014 [13]
Ejectile detector	SiRi ($\theta = 40.0\text{--}54.0^\circ$) [14]	SiRi ($\theta = 40.0\text{--}54.0^\circ$) [14]	SiRi ($\theta = 126.0\text{--}140.0^\circ$) [14]
γ -ray detector	NaI ($n_{\text{det}} = 23$) [15]	NaI ($n_{\text{det}} = 23$) [15]	NaI ($n_{\text{det}} = 26$) [15]
γ -ray efficiency (1.3 MeV)	$\approx 12.8\%$	$\approx 12.8\%$	$\approx 14.5\%$
Distance from target	22.0 cm	22.0 cm	22.0 cm
Target	$^{\text{nat}}\text{Si}$ (4 mg/cm 2)	$^{\text{nat}}\text{C}$ (1 mg/cm 2)	$^{\text{nat}}\text{C}$ (180 $\mu\text{g}/\text{cm}^2$)
$\epsilon_{1.78}$ (measured)	0.002307(3) $_{\text{stat.}}$ \times 1.00(3) $_{\text{syst.}}$ = 0.00231(7)		
$\epsilon_{3.20}$ (measured)	0.00141(1) $_{\text{stat.}}$ \times 1.00(3) $_{\text{syst.}}$ = 0.00141(5)		
$\epsilon_{4.44}$ (measured)		0.001267(3) $_{\text{stat.}}$ \times 1.00(3) $_{\text{syst.}}$ = 0.00127(4) $^{\text{a}}$	0.001352(1) $_{\text{stat.}}$ \times 1.00(3) $_{\text{syst.}}$ = 0.00135(4) $^{\text{a}}$

$^{\text{a}}$ In this work, the absolute photopeak efficiency (per detector) of CACTUS was determined as an uncertainty weighted average of $\epsilon_{4.44} = 0.00131(3)$.

excitation of the Hoyle state, *Physics Letters B* **827**, 136928 (2022).

- [9] K. C. W. Li, P. Adsley, R. Neveling, P. Papka, F. D. Smit, E. Nikolskii, J. W. Brümmer, L. M. Donaldson, M. Freer, M. N. Harakeh, F. Nemulodi, L. Pellegri, V. Pseudo, M. Wiedeking, E. Z. Buthelezi, V. Chudoba, S. V. Förtsch, P. Jones, M. Kamil, J. P. Mira, G. G. O’Neill, E. Sideras-Haddad, B. Singh, S. Siem, G. F. Steyn, J. A. Swartz, I. T. Usman, and J. J. van Zyl, Multiprobe study of excited states in ^{12}C : Disentangling the sources of monopole strength between the energy of the Hoyle state and $E_x = 13$ MeV, *Phys. Rev. C* **105**, 024308 (2022).
- [10] M. Tsumura, T. Kawabata, Y. Takahashi, S. Adachi, H. Akimune, S. Ashikaga, T. Baba, Y. Fujikawa, H. Fujimura, H. Fujioka, T. Furuno, T. Hashimoto, T. Harada, M. Ichikawa, K. Inaba, Y. Ishii, N. Itagaki, M. Itoh, C. Iwamoto, N. Kobayashi, A. Koshikawa, S. Kubono, Y. Maeda, Y. Matsuda, S. Matsumoto, K. Miki, T. Morimoto, M. Murata, T. Nanamura, I. Ou, S. Sakaguchi, A. Sakaue, M. Sferrazza, K. Suzuki, T. Takeda, A. Tamii, K. Watanabe, Y. Watanabe, H. Yoshida, and J. Zenihiro, First experimental determination of the radiative-decay probability of the 3_1^- state in ^{12}C for estimating the triple alpha reaction rate in high temperature environments, *Physics Letters B* **817**, 136283 (2021).
- [11] G. Cardella, F. Favela, N. S. Martorana, L. Acosta, A. Camaiani, E. De Filippo, N. Gelli, E. Geraci, B. Gnoffo, C. Guazzoni, G. Immè, D. J. Marín-Lámbarri, G. Lanzalone, I. Lombardo, L. Lo Monaco, C. Maiolino, A. Nannini, A. Pagano, E. V. Pagano, M. Papa, S. Pirrone, G. Politi, E. Pollacco, L. Quattrocchi, F. Risitano, F. Rizzo, P. Russotto, V. L. Sicari, D. Santonocito, A. Trifirò, and M. Trimarchi, Investigating γ -ray decay of excited ^{12}C levels with a multifold coincidence analysis, *Phys. Rev. C* **104**, 064315 (2021).
- [12] H. Fynbo, C. Diget, U. Bergmann, M. J. G. Borge, J. Cederkäll, P. Dendooven, L. M. Fraile, S. Franchoo, V. N. Fedosseev, B. R. Fulton, W. Huang, J. Huikari, H. B. Jeppesen, A. S. Jokinen, P. Jones, B. Jonson, U. Köster, K. Langanke, M. Meister, T. Nilsson, G. Nyman, Y. Prezado, K. Riisager, S. Rinta-Antila, O. Tengblad, M. Turrión, Y. Wang, L. Weissman, K. Wilhelmssen, J. Äystö, and T. I. Collaboration, Revised rates for the stellar triple-alpha process from measurement of ^{12}C nuclear resonances, *Nature* **433**, 136 (2005).
- [13] T. Kibédi, B. Alshahrani, A. E. Stuchbery, A. C. Larsen, A. Görge, S. Siem, M. Guttormsen, F. Giacoppo, A. I. Morales, E. Sahin, G. M. Tveten, F. L. B. Garrote, L. C. Campo, T. K. Eriksen, M. Klintefjord, S. Maharramova, H.-T. Nyhus, T. G. Tornyi, T. Renstrøm, and W. Paulsen, Radiative width of the Hoyle state from γ -ray spectroscopy, *Phys. Rev. Lett.* **125**, 182701 (2020).
- [14] M. Guttormsen, A. Bürger, T. Hansen, and N. Lietaer, The siri particle-telescope system, *Nuclear Instruments and Methods in Physics Research Section A: Accelerators, Spectrometers, Detectors and Associated Equipment* **648**, 168 (2011).
- [15] M. Guttormsen, A. Atac, G. Løvholden, S. Messelt, T. Ramsøy, J. Rekstad, T. F. Thorsteinsen, T. S. Tveter, and Z. Zelazny, Statistical gamma-decay at low angular momentum, *Physica Scripta* **1990**, 54 (1990).
- [16] F. Zeiser, G. Tveten, F. Bello Garrote, M. Guttormsen, A. Larsen, V. Ingeberg, A. Görge, and S. Siem, The γ -ray energy response of the oslo scintillator array oscar, *Nuclear Instruments and Methods in Physics Research Section A: Accelerators, Spectrometers, Detectors and Associated Equipment* **985**, 164678 (2021).
- [17] K. J. Cook, A. Chevis, T. K. Eriksen, E. C. Simpson, T. Kibédi, L. T. Bezzina, A. C. Berriman, J. Buete, I. P. Carter, M. Dasgupta, D. J. Hinde, D. Y. Jeung, P. McGlynn, S. Parker-Steele, B. M. A. Swinton-Bland, T. Tanaka, and W. Wojtaczka, High-precision proton angular distribution measurements of $^{12}\text{C}(p, p')$ for the determination of the $E0$ decay branching ratio of the Hoyle state, *Phys. Rev. C* **104**, 024620 (2021).

- [18] L. C. Biedenharn and M. E. Rose, Theory of angular correlation of nuclear radiations, *Rev. Mod. Phys.* **25**, 729 (1953).
- [19] D. R. Hamilton, On directional correlation of successive quanta, *Phys. Rev.* **58**, 122 (1940).
- [20] T. Kibédi, T. Burrows, M. Trzhaskovskaya, P. Davidson, and C. Nestor, Evaluation of theoretical conversion coefficients using bricc, *Nuclear Instruments and Methods in Physics Research Section A: Accelerators, Spectrometers, Detectors and Associated Equipment* **589**, 202 (2008).
- [21] T. K. Eriksen, T. Kibédi, M. W. Reed, A. E. Stuchbery, K. J. Cook, A. Akber, B. Alshahrani, A. A. Avaa, K. Banerjee, A. C. Berriman, L. T. Bezzina, L. Bignell, J. Buete, I. P. Carter, B. J. Coombes, J. T. H. Dowie, M. Dasgupta, L. J. Evitts, A. B. Garnsworthy, M. S. M. Gerathy, T. J. Gray, D. J. Hinde, T. H. Hoang, S. S. Hota, E. Ideguchi, P. Jones, G. J. Lane, B. P. McCormick, A. J. Mitchell, N. Palalani, T. Palazzo, M. Ripper, E. C. Simpson, J. Smallcombe, B. M. A. Swinton-Bland, T. Tanaka, T. G. Tornyi, and M. O. de Vries, Improved precision on the experimental $E0$ decay branching ratio of the Hoyle state, *Phys. Rev. C* **102**, 024320 (2020).
- [22] M. Shamsuzzoha Basunia, Nuclear data sheets for $a = 28$, *Nuclear Data Sheets* **114**, 1189 (2013).
- [23] Z. Luo, M. Barbui, J. Bishop, G. Chubarian, V. Z. Goldberg, E. Harris, E. Koshchiy, C. E. Parker, M. Roosa, A. Saastamoinen, D. P. Scriven, and G. V. Rogachev, Radiative decay branching ratio of the hoyle state, *Phys. Rev. C* **109**, 025801 (2024).
- [24] Cardella, Giuseppe, Bonasera, Aldo, Martorana, Nunzia, Simona, Acosta, Luis, De Filippo, Enrico, Geraci, Elena, Gnoffo, Brunilde, Guazzoni, Chiara, Maiolino, Concettina, Pagano, Angelo, Pagano, Emanuele, Vincenzo, Papa, Massimo, Pirrone, Sara, Politi, Giuseppe, Risitano, Fabio, Rizzo, Francesca, Russotto, Paolo, and Trimarchi, Marina, Potential experimental evidence of an efimov state in ^{12}C and its influence on astrophysical carbon creation, *EPJ Web Conf.* **279**, 03001 (2023).
- [25] P. Naidon and S. Endo, Efimov physics: a review, *Reports on Progress in Physics* **80**, 056001 (2017).
- [26] J. Bishop, G. V. Rogachev, S. Ahn, E. Aboud, M. Barbui, A. Bosh, J. Hooker, C. Hunt, H. Jayatissa, E. Koshchiy, R. Malecek, S. T. Marley, M. Munch, E. C. Pollacco, C. D. Pruitt, B. T. Roeder, A. Saastamoinen, L. G. Sobotka, and S. Upadhyayula, Evidence against the efimov effect in ^{12}C from spectroscopy and astrophysics, *Phys. Rev. C* **103**, L051303 (2021).